Study of molecular structure, chemical reactivity and H-bonding interactions in the cocrystal of nitrofurantoin with urea

NJC

PAPER

Study of molecular structure, chemical reactivity and H-bonding interactions in the cocrystal of nitrofurantoin with urea

Received 00th January 2017,
Accepted 00th January 2017

DOI: 10.1039/x0xx00000x

www.rsc.org/njc

E. Khan[a], A. Shukla[a], N. Jadav[b], R. Telford[c], A. P. Ayala[d], P. Tandon[a,*], V. R. Vangala[b,*]

Cocrystal of nitrofurantoin with urea ($C_8H_6N_4O_5$)·(CH_4N_2O), a non-ionic supramolecular complex, has been studied. Nitrofurantoin (NF) is a widely used antibacterial drug for the oral treatment of infections of the urinary tract. The characterization of the cocrystal of nitrofurantoin with urea (NF-urea) performed spectroscopically by employing FT-IR, FT- and dispersive-Raman and CP-MAS solid-state ^{13}C NMR techniques, along with quantum chemical calculations. With the purpose of having a better understanding of H bonding (inter- and intra- molecular) two different models (monomer and monomer + 3urea) of NF-urea cocrystal were prepared. The fundamental vibrational modes characterized depending on their potential energy distribution (PED). A combined experimental and theoretical wavenumber study proves the existence of the cocrystal. The presence and nature of H-bonds present in the molecules ascertained using quantum theory of atoms in molecules (QTAIM) and natural bond orbital (NBO) analysis. As HOMO-LUMO gap tells the reactivity of a molecule, this gap is more for the API than the cocrystal showing more reactivity for the cocrystal. Global descriptors calculated to understand the chemical reactivity of the cocrystal and NF. The local reactivity descriptors such as Fukui functions, local softness and electrophilicity indices analyses performed to determine the reactive sites within the molecule. The comparison between NF-urea (monomer) and NF shows that the cocrystal has improved overall reactivity, affected by increased intermolecular hydrogen bond strength. The docking studies revealed that the active sites (C=O, N-H, NO_2, N-N) of NF showed best binding energies of −4.89 kcal mol^{-1} and −5.56 kcal mol^{-1} for MUL and 1EGO toxin respectively, which are bacterial proteins of *Escherichia coli*. This cocrystal could potentially work as an exemplar system to understand the H-bond interaction in biomolecules.

1. Introduction

Cocrystals are a class of extremely useful materials, which have attracted much interest in recent years due to their future potential applications in the field of pharmacy and biomedical science. A pharmaceutical cocrystal is a crystalline supramolecular complex composed of multiple molecular components in a definite stoichiometric ratio, one being the drug (API), while the other is a benign, non-toxic 'coformer' molecule where the intermolecular interactions are non-covalent in nature [1-3]. Coformer may be an excipient or another drug [4]. This technology gives opportunity to improve the solubility, dissolution rate, bioavailability, hygroscopicity, and compressibility of the API thus increasing the number of forms of an API by modifying its structure without altering the pharmacological properties of the pure API [5-6]. Pharmaceutical cocrystals have been described for many drugs such as aspirin, acetoaminophen, ibuprofen, etc [2,4,7-9].

A group of drugs namely nitrofurans are usually used as antibiotics. They have a broad antimicrobial spectrum and are active against gram-positive as well as gram-negative bacteria. They have been widely used in the dairy, poultry and livestock production industries [10]. It is an oral antibiotic widely used to treat infections of urinary tract and also used as chronic treatment against recurrent infections. WHO has this medicine in its Model List of Essential Medicines [11]. NF is active against some gram positive organisms such as *Staphylococcus epidermidis*, *Enterococcus faecalis*, *Staphylococcus agalactia*, group D streptococci, viridians streptococci and Corynebacterium [12,13]. Its spectrum of activity against gram negative organisms includes *E. coli*, Enterobacter, Neisseria, Salmonella and Shigella [12].

Density functional theory (DFT) is the most accepted theoretical approach for determining the electronic structures of polyatomic systems [14]. DFT has been comprehensively and fruitfully used to tackle all sorts of problems in materials science, molecular biology, condensed matter physics and numerous other areas [15-16].

In the present study, cocrystal of NF with urea has been studied in which NF is an API and urea a coformer. Different cocrystals of NF have already been synthesized in order to improve the physicochemical properties of NF [17]. Urea helps in the metabolism of nitrogen-containing compounds by animals, and also the urine of mammals have urea as the main nitrogen-containing substance. It is non-toxic and highly soluble in water (neither

[a] Department of Physics, University of Lucknow, Lucknow 226 007, India.
E-mail: poonam_tandon@yahoo.co.uk, tandon_poonam@lkouniv.ac.in;
Fax: +91 522 2740840; Tel: +91 522 2782653

[b] Centre for Pharmaceutical Engineering Science and School of Pharmacy and Medical Sciences, University of Bradford, Bradford, West Yorkshire, BD7 1DP, UK
Email: V.G.R.Vangala@bradford.ac.uk; Tel: +44 1274236116

[c] School of Chemistry and Biosciences, University of Bradford, Bradford, West Yorkshire, BD7 1DP, UK.
[d] Departamento de Física, Universidade Federal do Ceará, Fortaleza, Brazil
† Electronic Supplementary Information (ESI) available. See DOI: 10.1039/x0xx00000x

alkaline nor acidic). NF-urea cocrystal belongs to monoclinic crystal system and space group $P2_1/c$. The crystallographic study divulges that the lattice parameters are a = 6.6779(13) Å, b = 13.648(3) Å and c = 14.003(4) Å; α = 90 °, β = 110.95(3) and γ = 90 [17].

A vibrational spectroscopic investigation is an advantageous analytical tool for providing information of molecular systems at microscopic level. In present study, a complete vibrational analysis of NF-urea cocrystal has been performed by combining Raman and infrared (IR) data with quantum chemical calculations using DFT approach [18]. NF exists in both anhydrous (α- and β-forms) and hydrate (Forms I and II) polymorphic forms. The β-form of NF is a solid and more stable at room temperature. The crystallographic structure of cocrystal, which is used here is prepared by β-polymorphic form of NF with urea and this β-form of NF is commercially available in the market and used as a drug [17]. Zhang et al. [19] have used density functional calculations (B3LYP/6-31g(d,p)) to interpret the Terahertz Spectra on NF-urea. They only compared the THz Spectroscopy results with DFT results. To the best of our knowledge, no detailed vibrational analyses, or theoretical DFT calculations, have been performed on this form of NF-urea. Therefore, in this work, an attempt has been made to explore the uses of DFT to investigate the ground state optimized structure, ground-state electronic properties, HOMO-LUMO energy gap and chemical reactivity of NF-urea. With the purpose of improving the vibrational assignments by incorporating all the possible nearest neighbour H-bond interactions, a little bit bigger model of cocrystal (monomer + 3urea) has been made in which three additional urea molecules are attached to NF-urea (1:1). To validate idea of gaseous phase, calculations have been performed on 1:1 ratio and results were compared with the experimental. In order to obtain a quantitative as well as qualitative interpretation of the infrared and Raman spectra, the calculated vibrational spectra of NF-urea (monomer) and NF-urea (monomer + 3urea) were analysed on the basis of the potential energy distribution (PED). To understand the H-bond pattern both DFT and spectroscopic methods are used. Quantum theory of atom in molecules (QTAIM) and natural bond analysis (NBO) have been used to investigate the nature and potency of intermolecular H-bonding.

2. Experimental details

Nitrofurantoin (β-form) and urea were purchased from Sigma-Aldrich and used as received. The solvent used was of chromatographic grade. Nitrofurantoin (β-form, 2 mmol) and stoichiometric amount of urea (2 mmol) was dissolved in 160 mL of methanol at 70 °C and allowed to evaporate at ambient conditions for two days to produce yellow needles of 1:1 NF-urea cocrystal [17].

Bruker TENSOR 27 FT-IR spectrometer was used to collect the infrared spectrum of NF-urea cocrystal in the region 400-4000 cm^{-1}.

The transmission infrared spectra of NF and urea were also obtained using a FT-IR spectrometer (Bio-Rad, FTS 3000 MX IR spectrometer).

The FT-Raman spectrum of NF-urea cocrystal was recorded on a Bruker IFS 55 EQUINOX with Raman attachment which uses a 1064 nm Nd-YAG laser line as the excitation line for recording the Raman spectra in the region 20-3400 cm^{-1}, with a spectral resolution of 4 cm^{-1}; 512 scans were recorded with a laser power of 500 mW at the sample location.

The dispersive Raman microscope employed in the study of NF and urea was a JY Horiba LabRAM HR equipped with a confocal microscope, liquid-nitrogen-cooled charge-coupled device (CCD) and a multichannel detector (256 pixels x1024 pixels).

Cross-polarization Magic Angle Spinning (CP-MAS) solid state NMR spectra were acquired using a BrukerAvance III HD 400 MHz spectrometer fitted with a 4 mm HX-MAS BB/1H probehead.

3. Computational details

Firstly the optimized molecular structure, energy, and vibrational frequencies of NF-urea (monomer and monomer + 3urea) were calculated by using B3LYP density functional method [20-22]. The basis set 6-311++G(d,p) was used [23,24]. All the calculations for NF-urea were performed in the ground state with the Gaussian 09 software package [25].

Then the graphical formation of the calculated Raman and IR spectra were made using GaussView program provided by Gaussian 09 [25,26]. In order to visualise the molecular geometries from the Gaussian output file, GaussView and ChemCraft program were used [26,27]. The vibrational assignments of the normal modes were proposed on the basis of the PED calculated using the program Gar2Ped [28]. A complete set of 87 internal coordinates were defined using Pulay's recommendations [29]. Topological properties have been studied within the framework of the QTAIM [30] using the AIM2000 and AIMALL software [31, 32]. The electronic transition of molecules were calculated in the gas phase using the time dependent (TD)-DFT/6–311++G(d,p) method [33].

4. Result and discussion

4.1. Geometry optimization and energies

The crystal structure of NF, urea and NF-urea cocrystal is already known and structure of NF-urea (monomer) and NF-urea (monomer + 3urea) was obtained from the crystallographic data of NF-urea cocrystal [17]. All the four molecules were optimized and the optimized geometry of the ground state of the NF-urea (monomer), NF-urea (monomer + 3urea), NF (monomer) and urea (monomer) with atomic numbering scheme are shown in Fig. 1, Fig. 2, Fig. S1 and Fig.S2(ESI†), respectively.

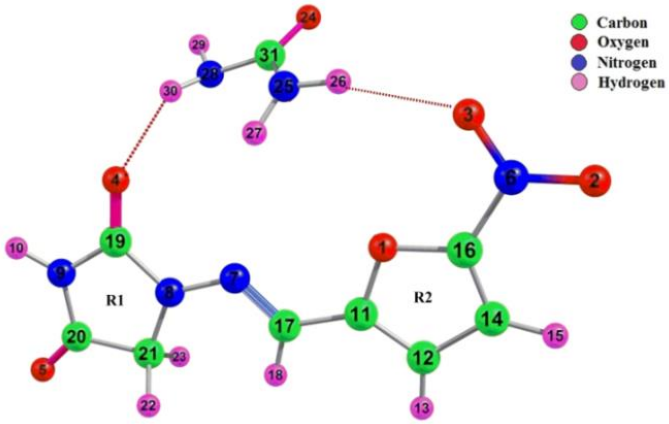

Fig. 1 Optimized structure for NF-urea (monomer).

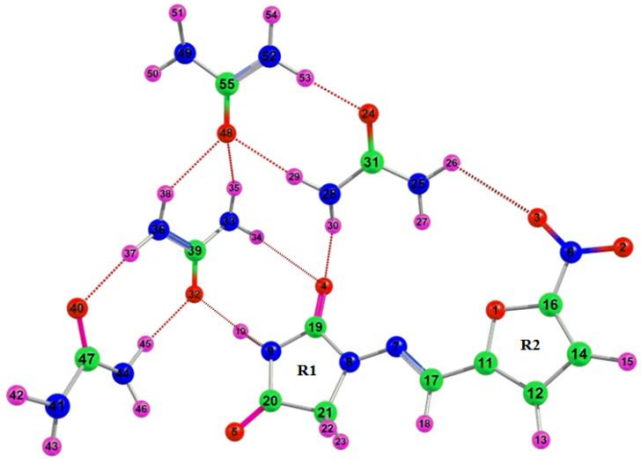

Fig. 2 Optimized structure for NF-urea (monomer + 3urea).

Optimized geometrical parameters of NF, cocrystal (monomer and monomer + 3urea) calculated at B3LYP/6-311++G(d,p) level are tabulated in Table S1 (ESI†), together with the experimental values taken from the crystallographic data [17].

A comparison of the calculated values of NF-urea (monomer) with the calculated values of NF shows that the calculation are same within 0.005 Å in bond lengths, 0.5° in bond angles and 2.2° in dihedral angles. Minor variances are, however, noticeable in the lengths of O4-C19, N8-C19 and N9-C19 bond of the hydantoin ring where the calculated values of the NF-urea (monomer) are 1.2024, 1.3971 and 1.4007 Å, respectively, as against the calculated values of the NF 1.1964, 1.4043 & 1.4078 Å. These variations in the lengths of bonds O4-C19, N8-C19 and N9-C19 in the NF-urea (monomer) are due to the presence of a strong H-bond between oxygen atom of C=O4 present in hydantoin ring and hydrogen atom H30 of amine group present in urea, which results in the increment of the O4-C19 bond, simultaneously in the shortening of the N8-C19 and N9-C19 bond (these H-bonds are not present in API).

The optimized structural parameters (bond lengths, bond angles and dihedral angles) of the NF-urea (monomer) were also compared with the experimental results [17] (comparison shown in Table S1, ESI†). The geometrical parameters of cocrystal (monomer + 3urea) show better agreement with the experimental values than the NF-urea (monomer) as nearest neighbour intermolecular H-bonds are incorporated in the cocrystal (monomer + 3urea) model. A comparison of the bond angles with the crystallographic data [17] shows that calculation are able to replicate the experimental data within 3.0° in bond angles and 3.6° in dihedral angles, differences are, however, noticeable in the bond angles of N7-C17-H18 and C11-C17-H18 in NF and H26-N25-H27, H29-N28-H30 and H29-N28-C31 in urea molecule. The variation in these bond lengths and bond angles between the theoretical and experimental values [17] may be credited to the fact that the experimental results are obtainable in condensed phase, where the molecules have a significant interaction due to crystal packing and intermolecular H-bonding, whereas in theoretical calculations an isolated monomer (NF-urea) is considered in gas phase.

The ground state energy of the NF-urea (monomer and monomer + 3urea) calculated by DFT method are −1129.07 and −1805.19 Hartrees. In the NF-urea (monomer), intermolecular H-bonds were formed between NF and urea. The binding energy of the analysed NF-urea (monomer) was computed as the difference between the calculated energies of the two isolated molecules i.e. NF and urea and the calculated total energy of the monomer. The total energy of NF and urea are calculated as −903.71 and −225.35 a.u. respectively using DFT calculations. The total energy and binding energy of the NF-urea (monomer) were calculated as −1129.07 a.u. and −7.11 kcal/mol. The correction in the calculated hydrogen binding energy of NF-urea (monomer) formation has been done for the basis set superposition error (BSSE) using the standard counterpoise method [33] and it comes out to be −6.47 kcal/mol.

4.2. Vibrational Assignment

The total number of atoms (N) in urea and NF are 8 and 23 and it gives 18 and 63 (3N−6) normal modes, respectively. The theoretical and experimental vibrational wavenumbers of NF and urea and their assignments using PED are given in Table S2 and S3 (ESI†). In the monomer of NF-urea there are 31 atoms, which give 87 vibrational modes. DFT calculations yield Raman scattering amplitudes not the Raman intensities. So, the Raman scattering cross-sections, $\partial\sigma_j/\partial\Omega$, which are proportional to the Raman intensities may be calculated from the Raman scattering amplitude and predicted wavenumbers for each normal modes [34,35].

There are 159 vibrational modes in cocrystal (monomer + 3urea) as it has 55 atoms. The theoretical vibrational wavenumbers of the NF-urea (monomer and monomer + 3urea), and the experimental wavenumbers of NF, urea and NF-urea cocrystal, and their assignments using PED are given in Table S4 (ESI†). Comparison of calculated (scaled) and experimental IR and Raman spectra of NF and urea are given in Fig. S3, S4, S5 and S6 (ESI†).

The calculated Raman and IR intensities were used to convolute each predicted vibrational mode with a Lorentzian line shape (FWHM = 8 cm−1) to produce simulated spectra. Comparison among experimental IR for NF-urea cocrystal, NF and urea and theoretical IR spectra for NF-urea (monomer and monomer + 3urea) in the region 3600-400 cm−1 is shown in Fig. 3. Calculated (scaled) Raman spectrum of the NF-urea (monomer and monomer + 3urea) and experimental Raman spectra of NF-urea cocrystal, NF and urea is shown in Fig. 4.

4.3. Vibrational wavenumbers and spectra

The calculated vibrational wavenumbers obtained from the DFT calculations are known to be greater than their experimental wavenumbers for the bulk of the normal modes, firstly, due to the environment (gas and solid phase) and secondly due to negligence of anharmonicity effects present in a real system. Therefore, calculated wavenumbers are scaled down by 0.9679 [36], to discard the anharmonicity present in real system [37,38]. Table 1 displays the change in theoretical and experimental bond length and stretching wavenumber of bonds, which are involved in H-bonding.

The investigated molecule contains a carbonyl group attached to urea molecule. In general, C=O stretching vibrations give rise to absorption band in the region of 1870–1540 cm^{-1}. The stretching vibration of urea carbonyl group ($\nu_{C=O}$) is calculated at 1719 cm^{-1} in cocrystal (monomer) and at 1729 cm^{-1} in urea (Table S3, ESI†), whereas this is calculated at 1692 cm^{-1} in NF-urea (monomer + 3urea). Sinking in the wavenumber of carbonyl group is observed when comparison is done between coformer and cocrystal

(monomer + 3urea), this change is due to the formation of H-bond in case of NF-urea (monomer + 3urea) whereas it is free in urea resulting in the elongation of C=O by 0.0229 Å in NF-urea (monomer + 3urea). This stretching mode of urea is observed at 1690/1649 cm^{-1} in the IR/Raman spectrum of coformer.

The NH_2 asymmetric and symmetric stretching vibrations of urea are assigned at 3468 and 3340 cm^{-1}, respectively with very high intensity for asymmetric and medium intensity for symmetric vibrations. The NH_2 stretching vibration of cocrystal is assigned at 3364 cm^{-1}. A difference is observed in the wavenumber of N-H30 stretching when comparison is done between cocrystal and coformer. The downshifting in the wavenumber for NF-urea is because of H-bond present in cocrystal (N28-H30···O4) resulting in the elongation of N-H30 bond by 0.0018 Å and no such noticable

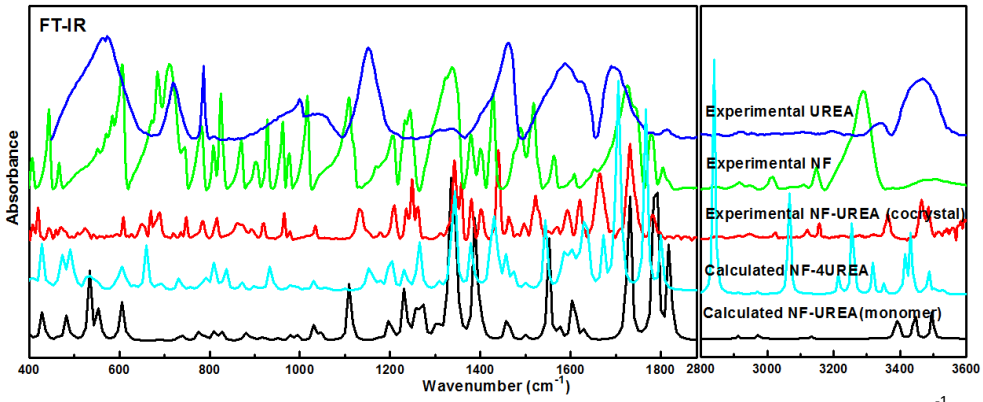

Fig. 3 Experimental FT-IR absorbance spectra of NF-urea, NF and urea in the region, 400-1900 and 2800-3600 cm^{-1} with the calculated IR spectra of NF-urea (monomer and monomer + 3urea).

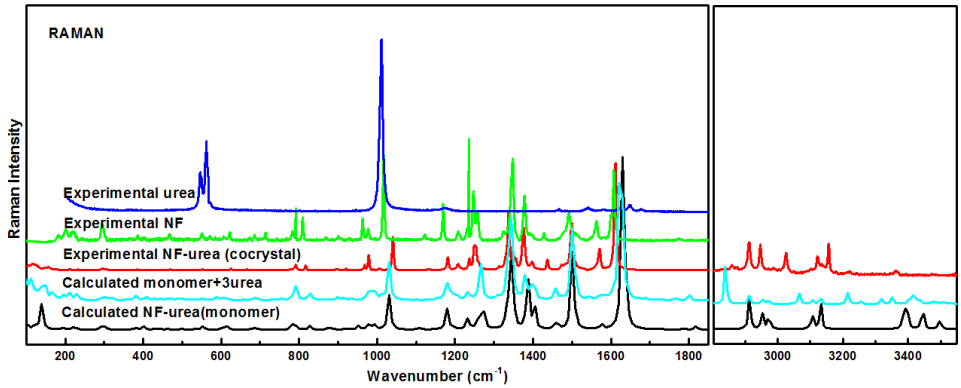

Fig. 4 Experimental Raman spectra of NF-urea, NF and urea in the region, 100-1850 and 2800-3600 cm^{-1} with the calculated Raman spectra of NF-urea (monomer and monomer + 3urea).

Table 1 The experimental and theoretical bond length (Å) and stretching frequency (cm^{-1}) of the bonds involved in hydrogen bonding.

Molecules	Groups present in NF									Groups present in urea					
	N-H group			C=O group			NO_2 group			NH_2 group			C=Ogroup		
	Bond length	Stretching frequency		Bond length	Stretching frequency		Bond length	Stretching frequency		Bond length	Stretching frequency		Bond length	Stretching frequency	
		IR	Raman		IR	Raman		IR	Raman		IR	Raman		IR	Raman
Experimental															
NF	0.9259	3287	-	1.2097	1830	-	1.2313	1520	1562	-	-	-	-	-	-
	-	-	-	1.2091	1780	-	1.2335	1342	1348	-	-	-	-	-	-
Urea	-	-	-	-	-	-	-	-	-	0.8980	3468	-	1.2502	1690	1649
	-	-	-	-	-	-	-	-	-	0.9023	3340	-	-	-	-
NF-urea	0.9259	3466	-	1.2097	1782	1781	1.2313	1549	1571	0.8980	3466	-	1.2502	1732	1781
	-	-	-	1.2091	1732	-	1.2335	1342	1334	1.2502	3364	-	-	-	-
Theoretical															
NF (monomer)	1.0103	3513	3513	1.1964	1811	1811	1.2225	1550	1550	-	-	-	-	-	-
	-	-	-	1.2041	1771	1771	1.2310	1527	1527	-	-	-	-	-	-
Urea (monomer)	-	-	-	-	-	-	-	-	-	1.0091	3571	3571	1.2167	1729	1729
	-	-	-	-	-	-	-	-	-	1.0088	3464	3464	-	-	-
NF-urea (monomer)	1.0106	3511	3511	1.2024	1800	1800	1.2249	1528	1528	1.0109	3566	3566	1.2220	1719	1719
	-	-	-	1.2022	1768	1768	1.2276	1320	1320	1.0082	3444	3444	-	-	-
NF-urea (monomer + 3urea)	1.0486	2862	2862	1.2075	1781	1781	1.2266	1520	1520	1.0116	3497	3497	1.2396	1692	1692
	-	-	-	1.2083	1746	1746	1.2288	1316	1316	1.0149	3374	3374	-	-	-

increment is observed in case of N-H29 bond as it is free in both cocrystal (monomer) and coformer (monomer). Both N-H29 and N-H30 bonds in NF-urea (monomer + 3urea) show increment in bond length by 0.0025 and 0.0061 Å with red shifting in wavenumber, proofing that both the bonds are H-bonded (Table 1).

In FT-IR spectrum of NF-urea cocrystal, the N-H stretch is observed at 3466 cm^{-1} and calculated as 3511/3513 cm^{-1} in cocrystal (monomer)/API (monomer) and at 2862 cm^{-1} in case of NF-urea (monomer + 3urea) (Table S4, ESI†) [39]. In API (monomer) and NF-urea (monomer) this N-H group is free whereas it is H-bonded in case of NF-urea (monomer + 3urea), so a red shift is calculated in the wavenumber of NF-urea (monomer + 3urea) with the increment in the bond length by 0.0383 Å. No such extension is observed in the bond length of NF and NF-urea (monomer).

The C=O stretching vibration is calculated to be 1800 cm^{-1} and 1811 $cm^{-1}$for NF-urea (monomer) and API (monomer) respectively corresponding to observed peak 1782 and 1830 cm^{-1} in IR spectrum of cocrystal and API, respectively. On moving from API to cocrystal in the FT-IR spectrum, a shifting of 48 cm^{-1} towards lower wavenumber side is observed, as expected, thus exhibiting standard behaviour. The lowering in the wavenumber specified that C=O4 group is involved in intermolecular H-bonding with H30. Red shift in the wavenumber and increment in the bond length is also observed in case of NF-urea (monomer + 3urea) because of the H-bond O4···H30 (Table 1).

In NF-urea (monomer and monomer + 3urea), O3 atom of NO_2 group is involved in H-bonding. In the FT-IR spectrum of NF-urea cocrystal, the NO_2 stretch is observed at 1549 cm^{-1}, although it is calculated to be 1550, 1528 and 1520 cm^{-1} in NF, NF-urea (momomer) and NF-urea (monomer + 3urea), respectively. This downshift in the wavenumber from API to NF-urea (monomer + 3urea) is attributed to the increase in the bond length of N-O3 from API to cocrystal (monomer + 3urea) by 0.0041 Å.

4.4. AIM calculations: Geometrical and topological parameters for multiple interactions

With the purpose of having an insight into H-bond interactions of a molecular system, QTAIM method has been applied. Geometrical and topological parameters are very useful means to exemplify the strength of H-bond. The bond critical point (BCP) is the point on the bond path at which the electron density, $\rho(r_{BCP})$ (minimum along the path) has lowest value. The geometrical requirements for the existence of H-bond are based on: (i) the distance between proton (H) and acceptor (A), is less than the sum of their van der Waal's radii of these atoms. (ii) The 'donor (D)-proton (H)···acceptor (A)' angle is greater than 90̊. (iii) The elongation of 'donor (D)-proton (H)' bond length is observed.

The existence of H-bond could be aided further by Koch and Popelier criteria [41] based on 'Atoms in Molecules' theory. According to Rozas et al. [42] these H-bond interactions may be categorized as follows: (i) Strong H-bonds are characterized by Laplacian of electron density ($\nabla^2\rho_{BCP}$)< 0 and total electron energy density (H_{BCP}) < 0 and their covalent character is established, (ii) Medium H-bonds are characterized by ($\nabla^2\rho_{BCP}$) > 0 and H_{BCP} < 0 and their partially covalent character is established and (iii) Weak H-bonds are characterized by ($\nabla^2\rho_{BCP}$) > 0 and H_{BCP}> 0 and they are mostly electrostatic in nature and the distance between interacting atoms is less than the sum of van der Waal's radii of these atoms. The van der Waals interactions are characterized by ($\nabla^2\rho_{BCP}$) > 0 and H_{BCP}> 0 and the distance between interacting atoms is greater than the sum of van der Waal's radii of these atoms.

The molecular graph of NF-urea (monomer and monomer + 3urea) using AIM program at B3LYP/6-311++G(d,p) level is presented in Fig.S9(ESI†) and Fig. 5 respectively. The calculated topological, geometrical and energy parameters for intermolecular H-bonds of interacting atoms of cocrystal (monomer + 3urea) are given in Table S5 (ESI†). The geometrical parameters for H-bonds of cocrystal (monomer + 3urea) are given in Table S6(ESI†). In cocrystal (monomer + 3urea), all the H-bonds have electron density in the range 0.0020–0.0400 a.u., except O32···H10, O1···H27 and N7···H27 which are not within the range predicted by Koch and Popelier criteria [41]. The bond O32···H10 has the smallest bond length as given in Table S5 (ESI†), so it is a very strong intermolecular H-bond, conversely the distance between the interacting atoms of H-bonds O1···H27 and N7···H27 is greater than the sum of van der Waal's radii of these atoms, so these two are very weak H-bonds. On the basis of these parameters, except above three bonds rest are medium H-bonds. At present, the QTAIM theory is used to estimate hydrogen bond energy (E). The relation between E and potential energy density (V_{BCP}) at H···O contact is E = 1/2(V_{BCP}) [43]. A number of interactions visualized in molecular graph are categorized on the basis of energetic parameters as follows:
O24···H53>O32···H45>O40···H37>O48···H35>O4···H30>O48···H29>O48···H38>O5···H46>O4···H34>O3···H26. The energy of these intermolecular H-bonds present in NF-urea (monomer + 3urea) and NF-urea (monomer) are listed in Table S5 and Table S7 (ESI†), respectively. According to AIM calculations, the binding energy of NF-urea (monomer) is sum of the energies of two intermolecular interactions (C=O4···H30 and N6-O3···H26) and is calculated as −6.02 kcal mol^{-1} which matches well with the binding energy calculated using DFT.

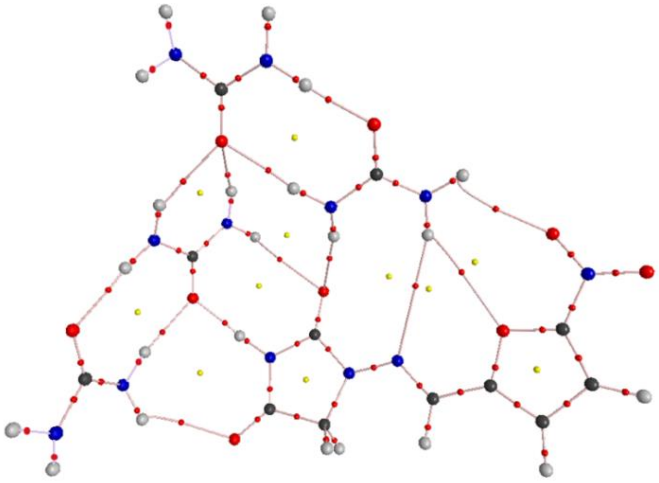

Fig. 5 Molecular graph of the NF-urea (monomer + 3urea): bond critical points (small red spheres), ring critical points (small yellow sphere), bond paths (pink lines).

4.5. NBO analysis

NBO analysis was originally developed as a way of quantifying resonance structure contributions to molecules. They are orbitals localized on typically one or more centers that are used to describe the Lewis-like molecular bonding pattern of electrons. A useful aspect of the NBOs is that it provides an accurate method for studying intra and intermolecular interaction and also gives an efficient basis for investigating charge transfer or conjugative interaction in various molecular systems [44].

The second order perturbation energy (E^2) values provide the strength of the donor-acceptor interaction based on all of the intuitive means for describing the interaction. It was done by examining all possible interactions between donor and acceptor orbitals, and calculating their stabilization energy by second order perturbation theory [45-47]. Therefore, the E^2 values can be considered as a good representation of the bond strength. In order to characterize the intra and intermolecular interactions quantitatively, a second-order perturbation theory is applied that gives the energy lowering associated with such interactions. The second-order perturbative estimate of "donor-acceptor" interactions in the NBO basis for the cocrystal has been summarized in Table S8. Here only those hyperconjugative interactions are discussed, which involved in the hydrogen bonding and show high stabilization energy.

The second-order perturbation theory analyses of the Fock Matrix, in the NBO basis for intermolecular interactions are presented in Table S9. In cocrystal (monomer + 3urea), charge transfer from urea unit (2) to urea unit (5) due to n(2)O24→ σ*N52-H53 stabilized the molecule up to 13.44 kcal/mol and confirms the presence of classical interaction N52-H53···O24. Another strong intermolecular charge transfer n(1)O32/n(2)O32→ σ*N9-H10 confirms the presence of intermolecular interaction (N9-H210···O32) and stabilized the molecule up to 13.60/5.39 kcal/mol.

The valence hybrids analyses of NBOs show that all the O-C and N-C bond orbitals are polarized towards the oxygen (73.09% at O), nitrogen (62.23% at N) atoms, although the N-O bond orbitals are polarized towards the oxygen atom (75.50% at O) (Table S10 ESI†). Thus, they comprise with the maximum electron density on the oxygen and nitrogen atom and accountable for polarity of the molecule.

4.6. ^{13}C NMR spectroscopy

The ^{13}C NMR chemical shifts of NF-urea, NF and urea were calculated with gauge-including-atomic-orbital (GIAO) method at B3LYP level [49]. The experimental ^{13}C NMR spectra of NF-urea, NF and urea are shown in Fig. 6, Fig. S10 and Fig. S11 (ESI†), respectively. The experimental and calculated ^{13}C NMR chemical shifts of NF-urea, NF and urea are listed in Table S11 (ESI†). A single peak is observed at 118.2 ppm for the carbons C12 and C14, as both have similar surroundings. Both are attached to single hydrogen, doubly bonded to a carbon atom and singly bonded to another carbon atom. Therefore both the carbon atoms absorb same energy and give a single peak at 118.2 ppm. Same is the case with C11 and C16. The correlation between the calculated and experimental chemical shifts are compared and the correlation graph found to follow the linear equation; y = mx + C, where x is the calculated 13C NMR chemical shifts (δ in ppm), m is the slope, y is the experimental 13C NMR chemical shifts (δ in ppm) and C is the constant. The value of correlation coefficient (R2) shows that there is a good agreement between experimental and calculated 13C NMR chemical shifts. The 13C NMR correlation graph of NF-urea and NF is shown in Fig. S12 (ESI†).

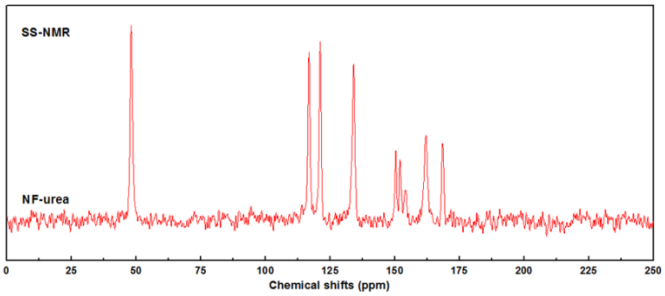

Fig. 6 Experimental 13C NMR spectrum of NF-urea.

4.7. Chemical Reactivity

4.7.1. Molecular Electrostatic Potential. The MEP map is widely used as a reactivity map displaying most probable regions for the electrophilic attack of charged point-like reagents on organic molecules [50-51].

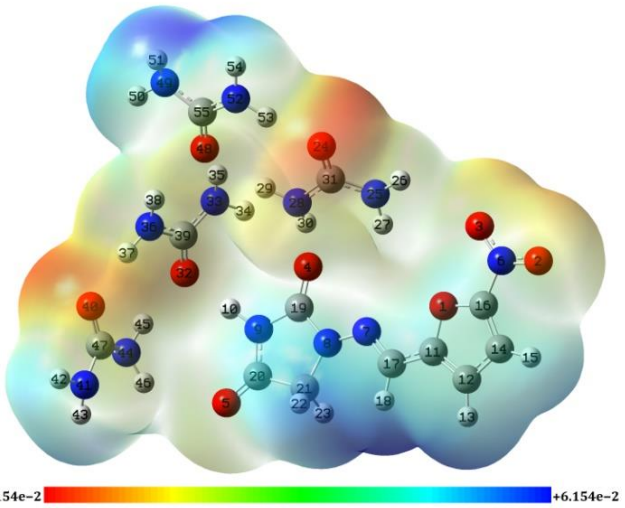

Fig. 7 Molecular electrostatic potential (MEP) formed by mapping of the total density over electrostatic potential in gas phase for NF-urea (monomer + 3urea).

The MEP of NF-urea (monomer + 3urea), NF-urea (monomer) and NF are presented in Fig. 7, Fig. S13 and Fig. S14 (ESI†), respectively. It is to be noted that the calculated MEP contour map shows the negative regions merely over moieties O2 and O3 atoms in both API and cocrystal, therefore, showing higher reactivity. Regions having positive potential are over the CH2 and N-H group of hydantoin ring. The region near the oxygen atom of carbonyl group (C=O24) of urea is most negative, in all three molecules while the regions near NH2 group of NF-urea (monomer + 3urea) are most positive as primary amines are nucleophilic in nature. Therefore, this MEP is very beneficial in explaining reactivity, hydrogen bonding and structure activity relationship of cocrystal.

4.7.2. HOMO–LUMO analysis. In agreement with the frontier molecular orbital theory, the creation of a transition state is the result of an interaction between the frontier orbitals (HOMO and

LUMO) of reactants [52]. Therefore, the energy difference between the HOMO and LUMO is a significant stability index. Smaller energy gap denotes higher electronic transition and vice versa.

The HOMO–LUMO energy gap (3.7092 and 2.9201 eV) of NF and NF-urea (monomer) molecule reflects the chemical stability of these molecules [53]. However, after the formation of cocrystal, the energy gap decreases (2.9201eV) which represents higher electronic transitions. The atomic molecular orbital plots for the frontier orbitals of NF and NF-urea are sketched in Fig. S15 (ESI†). High value of band gap signifies more stable the molecule, which further implies low reactivity [54]. The decrement in the value of the band gap from API to cocrystal shows that cocrystal (monomer) is chemically more reactive than API. In the case of NF-urea, the HOMO is localized almost on the coformer, whereas, the LUMO is localized on the nitro substituted furan ring, imide group and partially on hydantoin ring.

4.7.3. Molar Refractivity. Lipinski's rule of five evaluates the drug likeness or determines if a chemical compound with a definite biological or pharmacological activity has properties that would make it a likely orally active drug in humans [55]. In an attempt to improve the predictions of drug likeness, the rules have spawned many extensions. Out of these improved rules, three of them states that the compound should have:(i) Molar refractivity from 40 to 130, (ii) Molecular weight from 180 to 500, and (iii) Number of atoms from 20 to 70.

It is the MR value, which is responsible for the binding property and lipophilicity of the studied system. It may be calculated by the Lorenz-Lorentz formula [56-58]. The value of MR for NF-urea is 48.55 esu. The number of atoms and molecular weight of NF-urea (monomer) are 31 and 298.22 g/mol, respectively. Thus, the cocrystal satisfies above mentioned three properties which determine the drug likeness of a compound. As a result, cocrystal may be used as an orally active drug.

4.7.4. Electronic reactivity descriptors

4.7.4.1. Global reactivity descriptors. Electronegativity (χ), chemical potential (μ), global hardness (η), global softness (S) and electrophilicity index (ω) these all are global reactivity descriptors, exceptionally effective in predicting global reactivity trends. Global reactivity descriptors determined on the basis of Koopman's theorem, [59, 60] using the energies of frontier molecular orbitals ε_{HOMO}, ε_{LUMO} are given by equations. [61-66].

$$\chi = -\frac{1}{2}(\epsilon_{HOMO} + \epsilon_{LUMO})$$

$$\mu = -\chi = \frac{1}{2}(\epsilon_{HOMO} + \epsilon_{LUMO})$$

$$\eta = \frac{1}{2}(\epsilon_{LUMO} - \epsilon_{HOMO})$$

$$\omega = \frac{\mu^2}{2\eta}$$

$$S = \frac{1}{2\eta}$$

ω is a global reactivity index similar to the chemical hardness and chemical potential [65]. The value of ω measures the stabilization in energy when the system attains an additional electronic charge (ΔN) from the surroundings.

The energies of frontier molecular orbitals, energy band gap, χ, μ, η, S and ω for API, coformer, cocrystal (monomer and monomer + 3urea) are listed in Table 2. When two molecules react, the value of electrophilicity index determines which one will act as an electrophile (nucleophile). One can correlate the stability of the molecule to softness, the lower stability indicates that the molecule is softer and chemically more reactive [67]. As given in Table 2, where the value of η is high for API and the value S is high for cocrystal. So, the chemical reactivity of NF-urea (monomer) is higher than NF. The results suggest that cocrystals can be a feasible alternative for positively changing the targeted physicochemical properties of an active pharmaceutical ingredient (API).

Table 2 Calculated ε_{HOMO}, ε_{LUMO}, energy band gap ($\varepsilon_L - \varepsilon_H$), chemical potential ($\mu$), electronegativity ($\chi$), global hardness ($\eta$), global softness ($S$) and global electrophilicity index (ω) at 298.15 K for NF, urea, NF-urea (monomer and monomer + 3urea).

Molecule	ε_H (eV)	ε_L(eV)	$\varepsilon_L - \varepsilon_H$ (eV)	χ (eV)	μ (eV)	η (eV)	S (eV^{-1})	ω (eV)	ΔN_{max}
NF (monomer)	−7.0140	−3.3048	3.7092	5.159	−5.1594	1.8546	0.2696	7.1766	2.7819
Urea (monomer)	−7.3792	−0.6765	6.7027	4.028	−4.0279	3.3514	0.1492	2.4205	1.2019
NF-urea (monomer)	−6.5492	−3.6292	2.9200	5.089	−5.0892	1.4600	0.3425	8.8698	3.4858
NF-urea (monomer +3urea)	−7.0238	−3.5312	3.4926	5.278	−5.2775	1.7463	0.2863	7.9746	3.0221

4.7.4.2. Electrophilicity based charge transfer (ECT) descriptors. ECT descriptors present how the charge transferred in a molecule (cocrystal). It [66] is the difference between the ΔN_{max} values of interacting molecules.

$$ECT = (\Delta N_{max})_A - (\Delta N_{max})_B,$$

where $(\Delta N_{max})_A = -\mu_A/\eta_A$ and $(\Delta N_{max})_B = -\mu_B/\eta_B$. If two molecules A and B are approaching each other then, charge flow from B to A, if ECT > 0 else charge flow from A to B, if ECT < 0. ECT is calculated as 1.5799 for reactant molecules NF (A) and urea (B) which indicates that charge flows from urea (coformer) to NF (API) during the formation of cocrystal (Table 2).

The low value of μ and high value of ω for NF also prefer its electrophilic behavior. In the same way, the high value of μ and low value of ω for urea prefer its nucleophilic behavior. Therefore, NF acts as electron acceptor and urea as electron donor.

4.7.4.3. Local reactivity descriptors. Local reactivity descriptors give the exact location for the electrophilic and neuclophilic site present in cocrystal for further reaction. Using Hirshfeld atomic charges of neutral, cation and anion state of monomer + 3urea, Fukui functions (f_k^+, f_k^-, f_k^0), local softnesses (S_k^+, S_k^-, S_k^0) and local electrophilicity indices (ω_k^+, ω_k^-, ω_k^0) are calculated[68]. Fukui functions are calculated using the following equations.

$$\text{For nucleophilic attack,} \quad f_k^+ = [q(N+1) - q(N)]$$

$$\text{For electrophilic attack,} \quad f_k^- = [q(N) - q(N-1)]$$

$$\text{For radical attack,} \quad f_k^0 = \frac{1}{2}[q(N+1) + q(N-1)]$$

The values of local reactivity descriptors calculated for all the atomic sites of cocrystal (monomer + 3urea), NF-urea (monomer) and NF are listed in Table S12, Table S13 and Table S14 (ESI†), respectively. As given in Table S12 and Table S13 (ESI†), O24 atom has the maximum values of all the three local electrophilic reactivity

descriptors (f_k^+, S_k^+, ω_k^+) which imply that this site is prone to nucleophilic attack whereas O2 is prone to electrophilic attack as it has maximum values of f_k^-, S_k^-, ω_k^-.

4.8. Docking

Molecular docking [69] calculations were done to estimate the binding affinity of the ligand with the bacterial protein of E. coli (gram negative organism). In biological system when cocrystal dissolves, coformer separates from API and only API binds with protein, so molecular docking study was done only for API not for cocrystal. AutoDock 1.5.4 software was used for all the docking simulation [70]. Glutaredoxin, Hu Alpha and ELAV-1 are few proteins of E. Coli. The PDB code of protein of Glutaredoxin chosen for docking are 1GRXA, 5CAX, 1EGOA and 2MZC. 1MULA and 3HI9 are the PDB codes of protein Hu alpha2 and ELAV, respectively. All the 3D crystal structure of proteins was taken from RSCB Protein Data Bank. The ligand (NF) used for docking studies was obtained by minimizing its energy at a B3LYP/6-311++G(d,p) level of theory. A grid of size 60Å×60Å×60Å was demarcated to define the active site of the enzyme which includes residues of the active site. The undesirable ligands and water molecules present in the protein were removed using Discovery Studio Visualizer 4.5 software [71]. The ligand binds at the active sites of the protein by weak non-covalent interactions (H-bonding). NF interacts with 3HI9 toxin by six hydrogen bonds and the interacting residues are Asn 21, Ser 48, Ala 49 and Arg 37 of chain A, Arg 35 of chain C. NF interacted with 1MULA by residue Ser 81 of chain A and the length of the bond formed was 2.14 Å. The ligand effectively binds with both 1MULA and 3HI9 toxin with minimum binding energies of −4.89 kcal mol−1 and −10.64 kcal mol−1 respectively. Fig. S16 showed the inhibitory activity of NF active compound against both the targets. NF interacts with one of the glutaredoxin protein by three hydrogen bonds and the interacting residues are ThrA 58, ThrA 73 and AspA 74 and its binding energy is −5.56 kcal mol^{-1}. Mostly all the interactions involved are between protein and hydantoin ring and NO_2 group of ligand. All the protein-ligand interactions are displayed in Fig. S17 and the H-bond length, residues and binding affinity values is given Table S15 (ESI†). The results given in Table S15 conclude that the compound exhibit inhibitive activity against E. Coli and may act as antibacterial drug.

5. Conclusion

A systematic study has been done on the structural and spectral characteristics of the NF-urea cocrystal by experimental spectroscopic methods and quantum chemical calculations on two models (monomer and monomer + 3urea). Interpretation of the changes occurring in the wavenumber of API and cocrystal has been done. Elongation in the bond lengths of the atoms involved in H-bonding is observed causing red shift in the wavenumber of stretching modes of corresponding bonds. The calculated C=O stretching mode of Ring 1 agrees better in NF-urea (monomer + 3 urea) than in NF-urea (monomer). Intermolecular hydrogen bonding between API and all four urea molecules, and consequent changes in bond lengths and vibrational wavenumbers of NH_2 group involved in hydrogen bonding were discussed. The theoretically calculated IR and Raman spectra of NF-urea (monomer + 3 urea) show good correlation with experimentally observed spectra of cocrystal as all the possible nearest neighbour interactions (more H-bonds) are considered in this model. The wavenumber calculated using DFT matches very well with the experimental values. AIM calculations suggest that the nature of the H-bonds present in the title molecule is moderate as ($\nabla^2\rho_{BCP}$) > 0 and H_{BCP}< 0. C=O24 and NH_2 group came out to be the most active site from MEP study. HOMO-LUMO calculations on all the three molecules (API, coformer and cocrystal) were performed, concluding that cocrystal (monomer) is chemically more reactive than API. Molar Refractivity value of NF-urea (monomer) also lies in the range set by Lipinski. Global electrophilicity index (ω = 8.8698 eV) shows that title molecule (NF-urea) is a strong electrophile and chemically softer than NF and urea. From the molecular docking study, it is clear that NF display inhibitive activity against E. Coli and may act as antibacterial drug. The present study may recommend that it may be plausible to design a new chain of drugs with appropriate substitution with improved biological and chemical activities.

Acknowledgement

All solid-state NMR spectra were obtained at the EPSRC UK National Solid-state NMR Service at Durham. E.K. is thankful to UGC, New Delhi for providing financial assistance under UGC-BSR fellowship. P.T. and A.S acknowledge the financial support provided by the DST, India under the Indo-Brazil project and DST-PURSE fellowship scheme. V.R.V. thanks University of Bradford for a start up funding.

References

[1] S. L. Childs, G. P. Stahly, A. Park, Mol. Pharmaceutics, 2007, 4, 323–338.
[2] P. Vishweshwar, J. A. McMahon, J. A. Bis, M. J. Zaworotko, J Pharm Sci, 2006, 95, 499-516.
[3] C. B. Aakeroy, D. J. Salmon, CrystEngComm, 2005, 7, 439-448.
[4] N. Rodríguez-Hornedo, J. Nehm, A. Jayasankar, Taylor & Francis, 2007, 3, 615-635.
[5] N. Schultheiss, A. Newman, Cryst Growth Des, 2009, 9, 2950.
[6] Ö. Almarsson, M. J. Zaworotko, ChemCommun, 2004; 1889.
[7] P. Vishweshwar,J. A. McMahon, M. L. Peterson, M. B. Hickey, T. R. Shattock, M. J. Zaworotko, ChemCommun, 2005, 4601-4603.
[8] N. J. Babu, L. S. Reddy, S. Aitipamula, A. Nangia, Chem Asian J, 2008, 3, 1122-1133.
[9] B. Sarma, L. S. Reddy, A. Nangia, Cryst Growth Des, 2008, 8, 4546-4552.
[10] R. Draisci, L. Giannetti, L. Lucentini, L. Palleschi, G. Brambilla, L. Serpe, P. Gallo, J. of Chromatography A, 1997, 777(1), 201-211.
[11] WHO model list of Essential Medicines. http://www.who.int/selectionmedicines/committees/expert/17/]sixteenth adult list en, 2011.
[12] Macrodantin package insert (Procter & Gamble—US), Rev 2/98, Rec 3/99.
[13] Macrobid package insert (Procter & Gamble—US), Rev 2/98, Rec 3/99.
[14] H. C. Stephen Chan, ab John Kendrick, a Marcus, A. Neumannc, Frank J. J. Leusen, CrystEngComm, 2013, 15, 3799.
[15] S. Ghosh, P. P. Bag, C. M. Reddy, Cryst Growth Des, 2011, 11, 3489-3503.

[16] K. Srivastava, M. R. Shimpi, A. Srivastava, P. Tandon, K. Sinha, S. P. Velaga, RSC advances, 2016, 6, 10024-10037.
[17] V. R. Vangala, P. S. Chow, R. B. H. Tan, Cryst. Growth Des., 2012,12, 5925-5938.
[18] P. Hohenberg, W. Kohn, Phys. Rev., 1964,136B, 864–871.
[19] Zhang, Qi Fang, Hongxia Zhang, Huili Qin, Dan Hong, Zhi Du, Yong, ActaChim. Sinica, 2015, 73, 1069-1073.
[20] C. T. Lee, W. T. Yang, R. G. Parr, Phys Rev., 1988, 37B, 785–789.
[21] R. G. Parr, W. Yang, Ann Rev Phys Chem., 1995, 46, 701–728.
[22] A. D. Becke, J Chem Phys., 98, 1993, 5648–5652.
[23] G. A. Petersson, M. A. Allaham. J Chem Phys., 1991, 94(9), 6081–6090.
[24] G. A. Petersson, A. Bennett, T. G. Tensfeldt, M. A. Allaham, W. A. Shirley, J. Mantzaris, J Chem Phys,1988, 89(4), 2193-2219.
[25] M. J. Frisch, G. W. Trucks, H. B. Schlegel, G. E. Scuseria, J. R. Cheeseman, M. A. Robb, G. Scalmani, V. Barone, B. Mennucci, G. A. Petersson, H. Nakatsuji, M. Caricato, X. Li, H. P. Hratchian, A. F. Izmzylov, J. Bloino, G. Zheng, J. L. Sonnenberg, M. Hada,M. Ehara, K. Toyota, R. Fukuda, J. Ishida, M. Hasegawa, T. Nakajima, Y. Honda, O. Kitao, H. Nakai, T. Vreven, J. A. Montgomery, J. E. Peralta Jr., F. Ogliaro,M. Bearpark, J. J. Heyd,E. Brothers, K. N. Kudin, V. N. Staroverov, R. Kobayashi, J. Normand, A. Raghavachari, A. Rendell, J. C. Burant, S. S. Iyengar, J. Tomasi, M. Cossi, N. Rega, J. M. Millan, M. Klene,J. E. Knox, J. B. Cross, V. Bakken, C. Adamo, J. Jaramillo, R. Gomperts, R. E. Stratmann, O. Yazyev, A. J. Austin, R. Cammi, C. Pomelli, J. W. Ochterski, R. L. Martin, K. Morokuma, V. G. Zakrzewski, G. A. Voth, P. Salvador, J. J. Dannerberg, S. Dapprich, A. D. Daniels, J. Farkas, B. Foresman, J. V. Ortiz, J. Cioslowski and D. J. Fox, GAUSSIAN 09, Revision, Gaussian, Inc., Wallingford CT, 2009.
[26] A. Frisch, A. B. Nielson, A. J. Holder, GaussView User Manual, Gaussian Inc, Pittsburgh, PA, 2005.
[27] G. A. Zhurko and D. A. Zhurko, Chemcraft, 2005, http://www.chemcraftprog.com.
[28] J.M.L. Martin, C. Van Alsenoy, Gar2ped, University of Antwerp, 1995.
[29] P. Pulay, G. Fogarasi, F. Pang, J.E. Boggs, J. Am. Chem. Soc., 1979, 101, 2550–2560.
[30] R.F.W. Bader, Atoms in Molecules A Quantum Theory, Oxford University Press, Oxford, 1990.
[31] R.F.W. Bader, J.R. Cheeseman, AIMPAC Ed, 2000.
[32] T. A. Keith, AIMALL.Version 090201 TK Gristmill Software. Overland Park, KS. USA; 2009. http://aimtkgristmillcom
[33] E. Runge, E.K.U. Gross, Phys. Rev. Lett., 1984, 52, 997.
[34] G.A. Guirgis, P. Klaboe, S. Shen, D.L. Powell, A. Gruodis, V. Aleksa, C.J. Nielsen, J.Tao, C. Zheng, J.R. Durig, J. Raman Spectrosc., 2003, 34, 322–336.
[35] P.L. Polavarapu, J. Phys. Chem., 1990, 94, 8106–8112.
[36] M.P. Andersson, P. Uvdal, J. Phys. Chem. A., 2005, 109, 2937.
[37] A.P. Scott, L. Radom, J. Phys. Chem., 1996, 100, 16502-16513.
[38] M.W. Wong, Chem. Phys. Lett., 1996, 256, 391–399.
[39] A. Shukla, E. Khan, K. Srivastava, K. Sinha, P. Tandon, V. R. Vangala, Cryst Eng Comm, 2017, 19, 3921.
[40]M.R. Anoop, P.S. Binil, S. Suma, M.R. Sundarsanakumar, S. Mary, H.T. Varghese, C.Y. Panicker, J. Mol. Struct., 2010, 969, 48-54.
[41] U. Koch, P. Popelier, J. Phys. Chem.A, 1995, 99, 9747.
[42] I. Rozas, I. Alkorta, J. Elguero, J. Am. Chem. Soc., 2000, 122, 11154.
[43] E. Espinosa, E. Molins, C. Lecomte, Chem. Phys. Lett., 1998, 285, 170.
[44] A. Chandran, H.T. Varghese, Y.S. Mary, C.Y. Panicker, T.K. Manojkumar, C.V. Alsenoy, G. Rajendran, Spectrochim. ActaA Mol. Biomol. Spectrosc.,2012, 92, 84-90.
[45] A. E. Reed, R. B. Weinstock, F. Weinhold, J. Chem. Phys., 1985, 83, 735.
[46] A. E. Reed, F. Weinhold, J. Chem. Phys., 1985, 83, 1736.
[47]A. E. Reed, L. A. Curtiss, F. Weinhold, Chem. Rev. (Washington, DC), 1988, 88, 899.
[48] N. Gonohe, H. Abe, N. Mikami, M. Ito, J. Phys. Chem., 1985, 89, 3642-3648.
[49]K. Wolinski, J.F. Hinton, J.F. Pulay, J. Am. Chem. Soc., 1990, 112, 8251-8260.
[50] D. J. Williams, Angew.Chem. Int. Ed. Engl., 1984, 23, 690.
[51] S. Moro, M. Bacilieri, C. Ferrari, G. Spalluto, Curr. Drug Discovery Technol., 2005, 2, 13-21.
[52] R.M. Issa, M.K. Awad, F.M. Atlam, Appl. Surf. Sci., 2008, 255, 2433–2441.
[53] K. Fukui, Science, 1982, 218, 747.
[54] E. Khan, A. Shukla, A. Srivastava, Shweta, P. Tandon, New J. Chem., 2015, 39, 9800-9812.
[55] C. A. Lipinski, F. Lombardo, B. W. Donimy, P. J. Feeny, Adv. Drug Delivery Reviews, 1997, 23, 3-25.
[56] J. A. Padro´n, R. Carasco and R. F. Pello´n, J. Pharm. Pharm. Sci., 2002, 5, 258–266.
[57] R. P. Verma and C. Hansch, Bioorg. Med. Chem., 2005, 13, 2355–2372.
[58] R. P. Verma, A. Kurup and C. Hansch, Bioorg. Med. Chem., 2005, 13, 237–255.
[59] R.G. Parr, W. Yang, Density Functional Theory of Atoms and Molecules, Oxford University Press, Oxford, New York, 1989.
[60] N.P.G. Roeges, A Guide to the Complete Interpretation of Infrared Spectra of Organic Structures, Wiley, New York, 1994.
[61] R.G. Pearson, J. Org. Chem., 1989, 54, 1430.
[62] R.G. Parr, R.G. Pearson, J. Am. Chem. Soc.,1983, 105, 7512.
[63] P. Geerlings, F. De Proft, W. Langenaeker, Chem. Rev., 2003, 103, 1793.
[64] R.G. Parr, L. Szentpaly, S. Liu, J. Am. Chem. Soc., 1999, 121, 1922.
[65] P.K. Chattaraj, U. Sarkar, D.R. Roy, Chem. Rev., 2006, 106, 2065.
[66] J. Padmanabhan, R. Parthasarathi, V. Subramaniaan, P.K. Chattaraj, J. Phys. Chem. A, 2007,111, 1358.
[67] K. Fukui, T. Yonezawa and H. Shingu, J. Chem. Phys.,1952, 20, 722.
[68] R.G. Parr and W. Yang, J Am Chem Soc., 1984,106, 4049-4050.
[69] A. Shukla, E. Khan, A. Srivastava, P. Tandon and K. Sinha, Mol. Simul., 2015, 2015, 42, 863-873.
[70] G.M. Morris, D.S. Goodsell, R.S. Halliday, R. Huey, W.E. Hart, R.K. Belew, A.J. Olson, J. Comput. Chem., 1998, 19, 1639-1662.
[71] Discovery Studio 4.5 Guide, Accelrys Inc., San Diego, http://www.accelrys.com, 2009.

Study of molecular structure, chemical reactivity and H-bonding interactions in the cocrystal of nitrofurantoin with urea

E. Khan[a], A. Shukla[a], N. Jadav[b], R. Telford[c], A. P. Ayala[d], P. Tandon[a,*], V. R. Vangala[b,*]

New Journal of Chemistry

†Electronic Supplementary Information

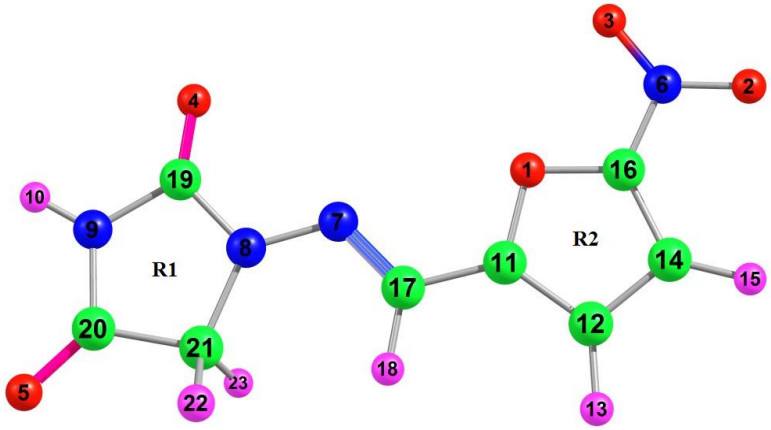

Fig.S1 Optimized structure for NF.

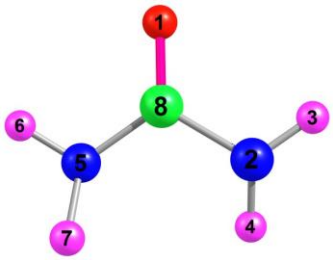

Fig. S2. Optimized structure for urea.

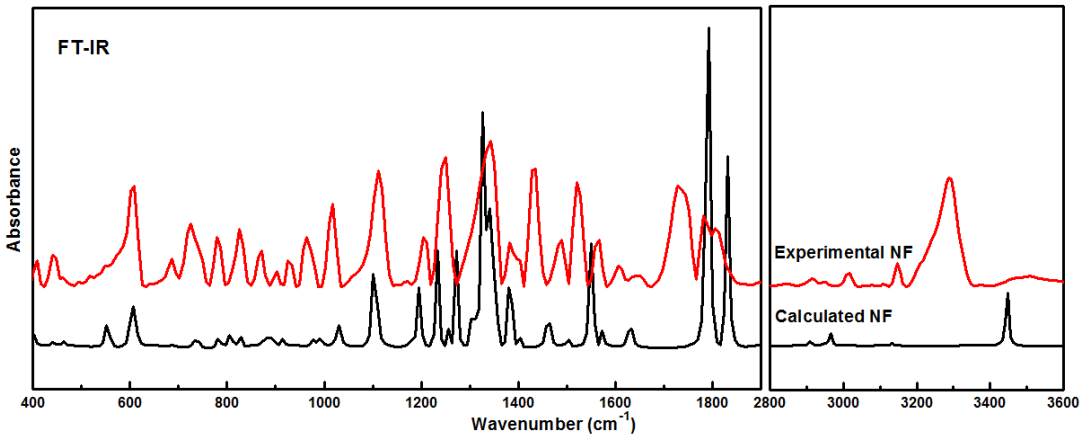

Fig. S3. Experimental and calculated FT-IR absorbance spectra of NF in the region, 400-3600 cm^{-1}.

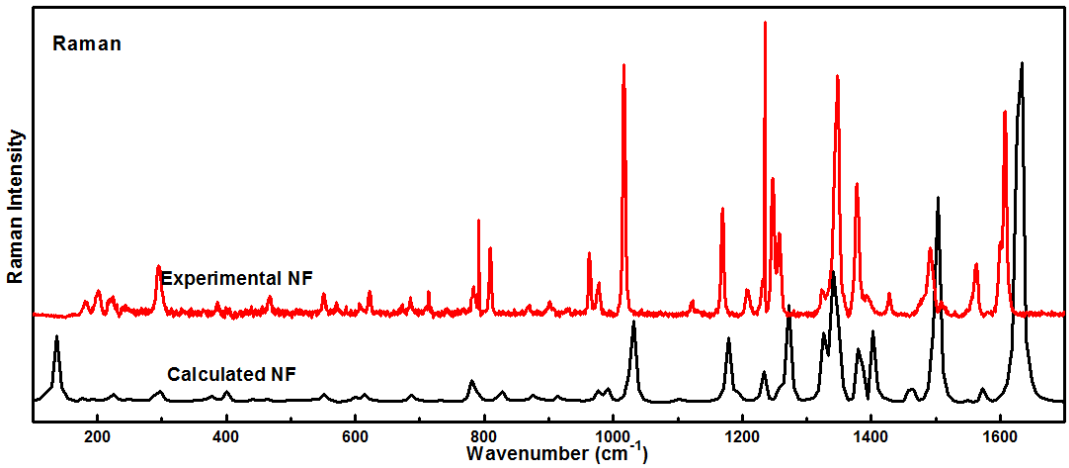

Fig. S4. Experimental and calculated Raman spectra of NF in the region, 100-1700 cm^{-1}.

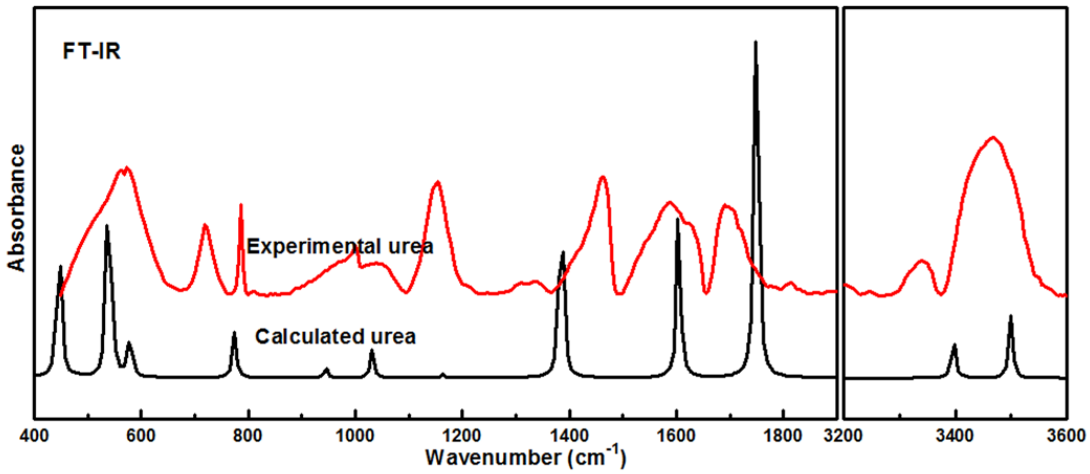

Fig. S5. Experimental and calculated IR absorbance spectra of urea in the region, 400-3600 cm^{-1}.

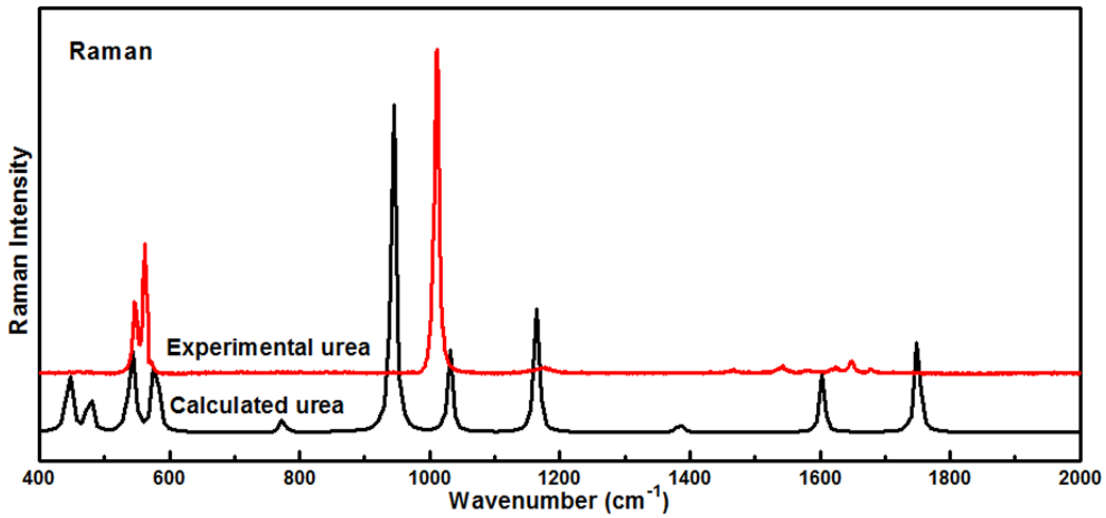

Fig. S6. Experimental and calculated Raman spectra of urea in the region, 400-2000 cm^{-1}.

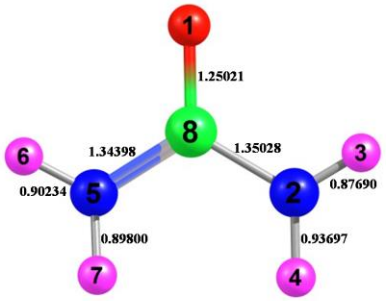

Fig. S7. Experimental structure of urea.

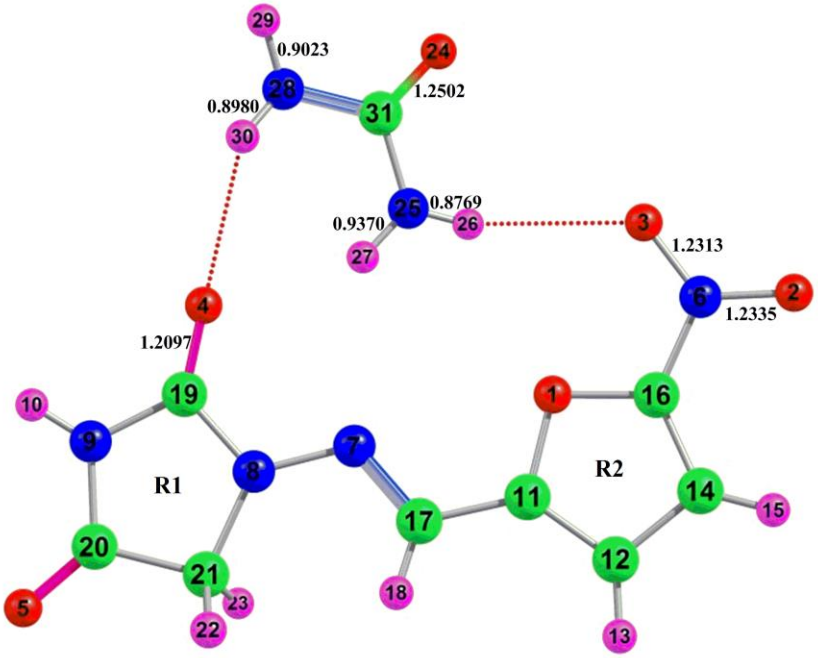

Fig. S8. Experimental structure of NF-urea.

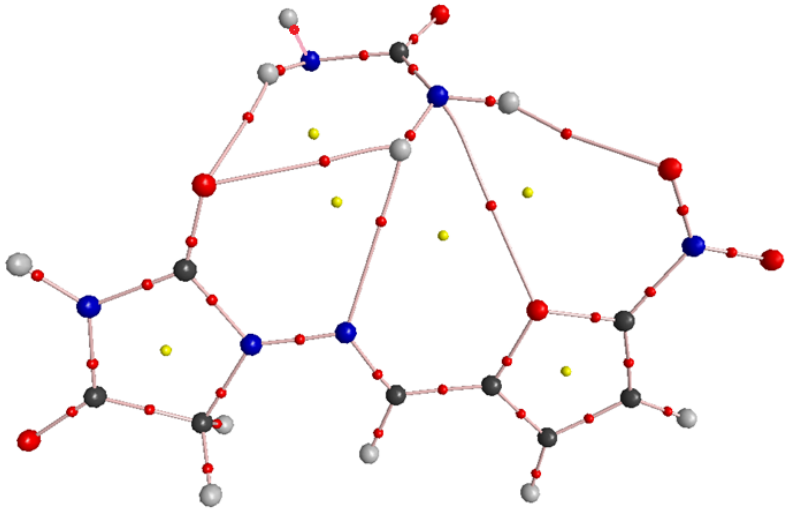

Fig. S9. Molecular graph of the NF-urea (monomer): bond critical points (small red spheres), ring critical points (small yellow sphere), bond paths (pink lines).

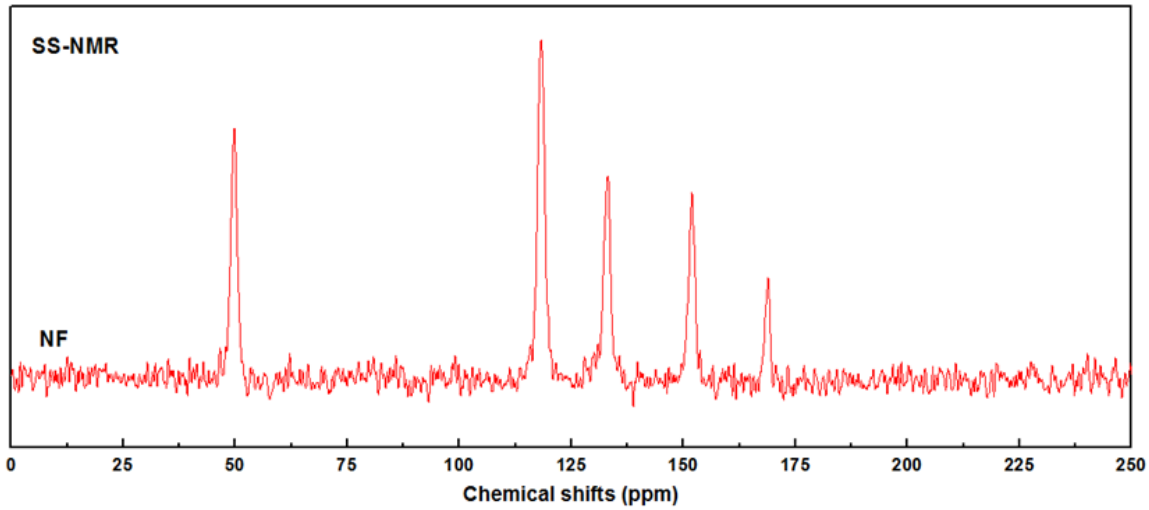

Fig. S10. Experimental ^{13}C NMR spectrum of NF.

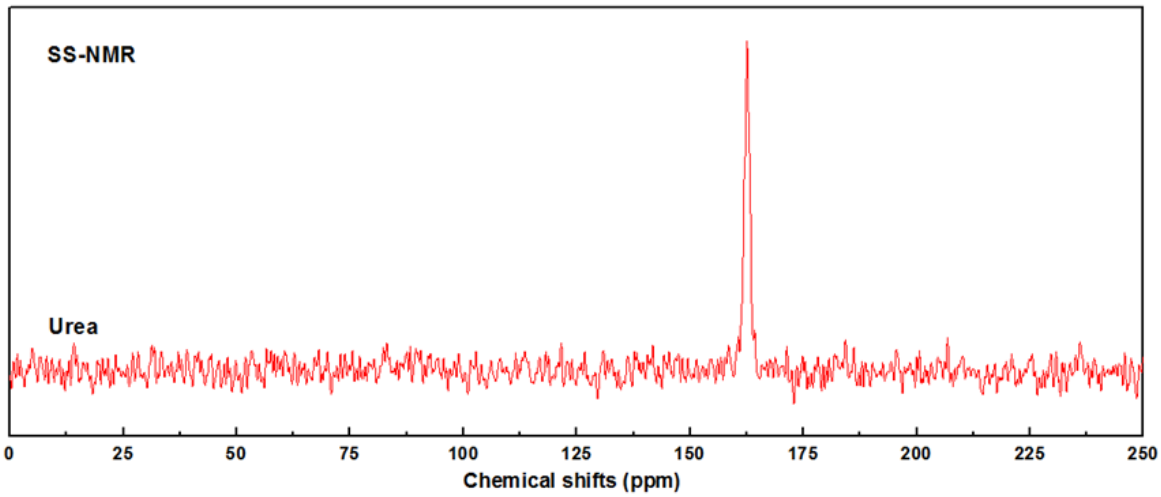

Fig. S11. Experimental ^{13}C NMR spectrum of urea.

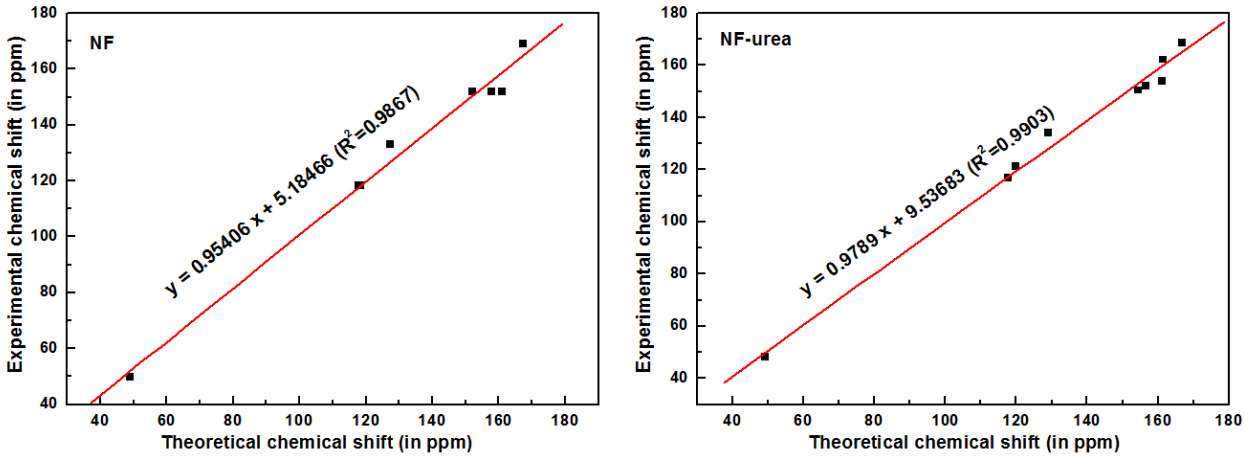

Fig. S12. The 13C NMR correlation graph of NF-urea and NF.

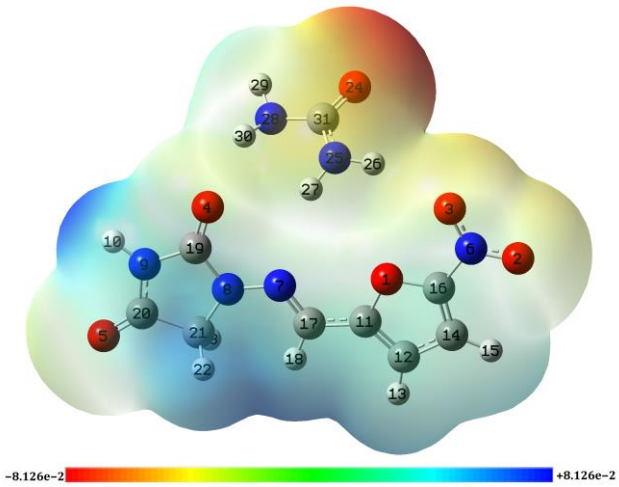

Fig. S13. Molecular electrostatic potential (MEP) formed by mapping of the total density over electrostatic potential in gas phase for NF-urea (monomer).

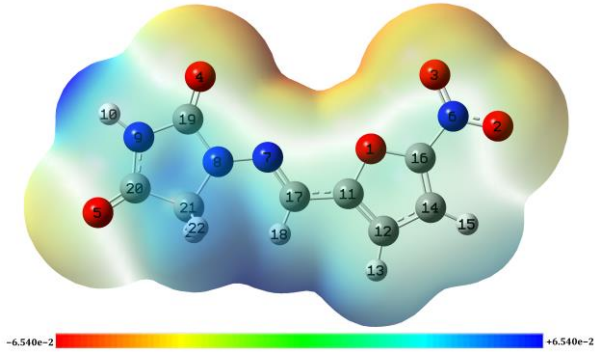

Fig. S14. Molecular electrostatic potential (MEP) formed by mapping of the total density over electrostatic potential in gas phase for NF.

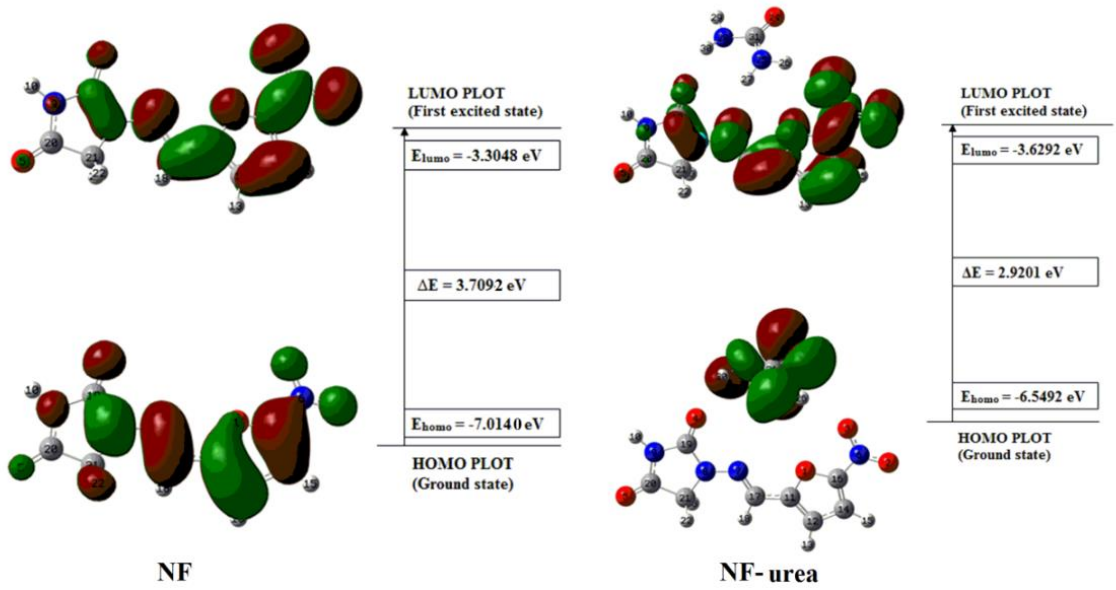

Fig. S15 HOMO-LUMO energy gap of NF and NF-urea (monomer) with orbitals involved in electronic transitions.

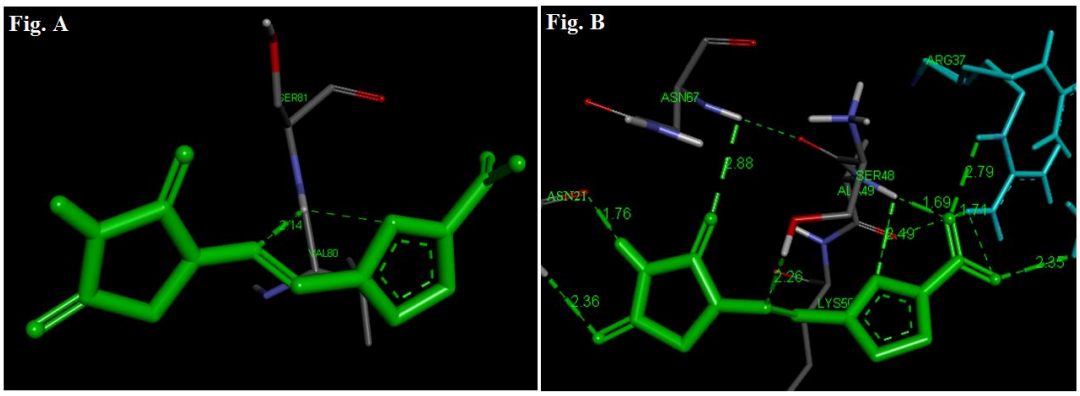

Fig. S16 The interaction of NF against drug targets- Hu Alpha2 Protein (1MULA)(Fig. A) and ELAV like protein 1 (3HI9)(Fig. B) generated by computer aided docking.

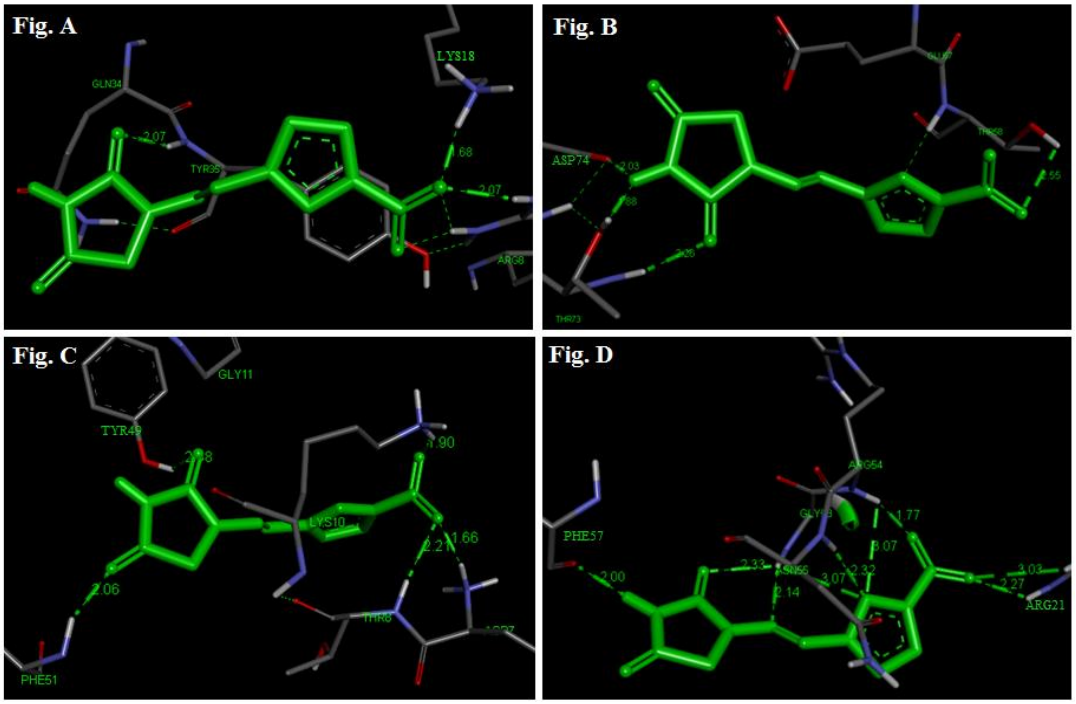

Fig. S17 The interaction of NF against drug targets-Glutaredoxin protein: 1GRXA (Fig. A), 1EGO (Fig. B), 5CAX (Fig. C) and 2MZC (Fig. D).

Table S1 The experimental and calculated geometric parameters of NF-urea and calculated geometric parameters of NF and NF-urea (monomer +3urea) using DFT/6-311++g(d,p), bond lengths in angstrom (Å) and bond angles in degrees (º).

Geometrical Parameters	Experimental	Calculated		
		Optimized parameters		
	NF-urea cocrystal	NF-urea (monomer + 3urea)	NF-urea (monomer)	NF (monomer)
		B3LYP/6-311++G(d,p)		
Bond lengths(Å)				
O1-C11	1.3748(19)	1.361	1.359	1.359
O1-C16	1.3564(19)	1.350	1.348	1.349
O2-N6	1.2334(18)	1.229	1.228	1.231
O3-N6	1.2313(18)	1.226	1.225	1.222
O4-C19	1.2100(2)	1.207	1.202	1.196
O5-C20	1.2093(19)	1.208	1.202	1.204
N6-C16	1.4220(2)	1.430	1.434	1.434
N7-N8	1.3605(18)	1.337	1.344	1.340
N7-C17	1.2870(2)	1.286	1.285	1.285
N8-C19	1.3800(2)	1.405	1.397	1.404
N8-C21	1.4542(19)	1.460	1.461	1.461
N9-H10	0.9259	1.049	1.010	1.010
N9-C19	1.3850(2)	1.387	1.401	1.408
N9-C20	1.3710(2)	1.373	1.381	1.377
C11-C12	1.3650(2)	1.379	1.378	1.379
C11-C17	1.4410(2)	1.442	1.441	1.442
C12-H13	0.9500	1.078	1.079	1.079
C12-C14	1.4170(2)	1.417	1.418	1.417
C14-H15	0.9500	1.077	1.077	1.077
C14-C16	1.3450(2)	1.365	1.365	1.365
C17-H18	0.9500	1.090	1.090	1.091
C20-C21	1.5210(2)	1.534	1.530	1.530
C21-H22	0.9900	1.095	1.094	1.094
C21-H23	0.9900	1.094	1.094	1.095
O24-C31	1.2503(19)	1.240	1.222	-
N25-H26	0.8764	1.006	1.008	-
N25-H27	0.9369	1.008	1.009	-
N25-C31	1.350(2)	1.366	1.372	-
N28-H29	0.9030	1.015	1.008	-
N28-H30	0.8980	1.012	1.011	-
N28-C31	1.3440(2)	1.364	1.390	-
Bond angle(°)				
C11-O1-C16	104.53(12)	106.24	106.19	106.19
O2-N6-O3	124.33(13)	125.83	126.03	126.04
O2-N6-C16	117.40(13)	116.09	115.89	115.67
O3-N6-C16	118.26(13)	118.08	118.07	118.29
N8-N7-C17	117.24(13)	119.65	118.97	119.022
N7-N8-C19	118.70(12)	119.25	119.50	119.76
N7-N8-C21	128.48(12)	128.38	128.13	127.83
C19-N8-C21	112.82(13)	111.46	112.36	112.40
H10-N9-C19	121.90	119.63	121.74	121.45
H10-N9-C20	125.50	125.58	124.05	124.03
C19-N9-C20	112.57(13)	113.21	114.21	114.51
O1-C11-C12	110.52(14)	109.96	110.02	110.05
O1-C11-C17	117.17(13)	119.08	119.41	119.79
C12-C11-C17	132.29(15)	130.95	130.57	130.16
C11-C12-H13	126.70	126.09	126.16	126.12

C11-C12-C14	106.65(14)	106.71	106.66	106.64
H13-C12-C14	126.70	127.20	127.18	127.24
C12-C14-H15	127.40	128.87	128.91	128.97
C12-C14-C16	105.18(14)	105.6	104.95	104.98
H15-C14-C16	127.40	126.06	126.13	126.05
O1-C16-N6	114.69(13)	117.35	117.25	117.63
O1-C16-C14	113.11(13)	112.03	112.16	112.14
N6-C16-C14	132.11(15)	130.61	130.58	130.23
N7-C17-C11	119.01(14)	120.22	121.10	121.20
N7-C17-H18	120.50	124.09	123.80	123.91
C11-C17-H18	120.50	115.69	115.10	114.88
O4-C19-N8	126.10(14)	126.66	128.12	128.68
O4-C19-N9	127.71(14)	126.87	126.66	126.65
N8-C19-N9	106.20(13)	106.46	105.22	104.67
O5-C20-N9	126.65(15)	127.77	127.45	127.59
O5-C20-C21	126.02(14)	125.65	126.96	126.77
N9-C20-C21	107.32(12)	106.58	105.59	105.63
N8-C21-C20	101.08(12)	102.17	102.62	102.78
N8-C21-H22	111.60	112.02	112.36	112.39
N8-C21-H23	111.60	112.74	112.38	112.37
C20-C21-H22	111.60	109.98	110.09	110.02
C20-C21-H23	111.60	110.42	109.97	110.01
H22-C21-H23	109.40	109.32	109.25	109.12
H26-N25-H27	120.90	117.23	116.86	-
H26-N25-C31	118.40	117.70	116.59	-
H27-N25-C31	120.70	122.00	120.38	-
H29-N28-H30	122.90	116.95	115.95	-
H29-N28-C31	117.70	116.24	113.27	-
H30-N28-C31	116.20	120.31	118.21	-
O24-C31-N25	121.54(15)	121.48	123.46	-
O24-C31-N28	121.37(14)	122.43	122.19	-
N25-C31-N28	117.08(14)	116.08	114.34	-
		Dihedral angle(°)		
C16-O1-C11-C12	0.44(17)	0.16	0.04	−0.0
C16-O1-C11-C17	179.01(13)	179.73	−179.90	179.99
C11-O1-C16-N6	−177.13(12)	-179.11	179.84	179.98
C11-O1-C16-C14	−0.21(17)	-0.07	−0.04	0.00
O2-N6-C16-O1	−178.70(13)	-17891	177.88	179.9
O2-N6-C16-C14	5.10(3)	2.26	−2.25	−0.07
O3-N6-C16-O1	2.30(2)	1.21	−2.02	−0.04
O3-N6-C16-C14	−173.86(16)	-177.63	177.84	179.92
C17-N7-N8-C19	178.02(13)	176.94	−179.00	−179.93
C17-N7-N8-C21	−1.80(2)	8.81	0.99	−0.07
N8-N7-C17-C11	179.46(13)	-178.30	−179.97	−180.00
N7-N8-C19-O4	−0.70(2)	8.16	0.72	−0.09
N7-N8-C19-N9	179.08(12)	-171.75	−179.35	179.92
C21-N8-C19-O4	179.16(15)	178.18	−179.27	−179.98
C21-N8-C19-N9	−1.070(17)	-1.73	0.65	0.03
N7-N8-C21-C20	−178.73(14)	168.58	179.34	−179.94
C19-N8-C21-C20	1.44(16)	-0.30	−0.66	−0.07
C20-N9-C19-O4	179.91(15)	-176.53	179.55	−179.97
C20-N9-C19-N8	0.15(17)	3.38	−0.37	0.02
C19-N9-C20-O5	179.97(15)	176.17	179.99	179.95
C19-N9-C20-C21	0.76(17)	-3.57	−0.03	−0.06
O1-C11-C12-C14	−0.50(18)	-0.19	−0.02	−0.00
C17-C11-C12-C14	−178.78(16)	-179.69	179.91	−180.00
O1-C11-C17-N7	1.90(2)	4.39	1.10	0.00

	C12-C11-C17-N7	−179.92(16)	-176.15	−178.83	180.00	
	C11-C12-C14-C16	0.35(18)	0.14	−0.00	0.01	
Table	C12-C14-C16-O1	−0.09(18)	-0.04	0.03	−0.01	**S2**
	C12-C14-C16-N6	176.15(16)	178.84	−179.84	−179.98	
	O5-C20-C21-N8	179.51(15)	-177.50	−179.62	−179.93	
	N9-C20-C21-N8	−1.27(15)	2.24	0.41	0.07	

Theoretical and experimental vibrational wavenumbers (cm^{-1}) of NF with PED.

Unscaled DFT	Scaled DFT	Raman	IR	Assignment
3630	3513	-	3503,3287	R1[υ(NH)](100)
3279	3174	-	3148	R2[υ(CH)](99)
3248	3144	-	3109	R2[υ(CH)](99)
3094	2995	-	3017	υ(CH)(99)
3077	2978	-	2947	R1[$\upsilon_a(CH_2)$](100)
3035	2937	-	2916	R1[$\upsilon_s(CH_2)$](49)
1871	1811	-	1830	R1[υ(C=O)(79)+δ'_{ring}(6)+υ(C19N)(9)]
1830	1771	-	1782	R1[υ(C=O5)(78)+υ(CN9)(7)
1660	1607	1608	1605	υ(CN7)(55)+ρ(CH)(15)+υ(CC)(15)+R2[υ(C11C12)](6)
1601	1550	1601	1566	R2[υ(CC)(45)+δ_{in}(CH)(9)]+$\upsilon(NO_2)$(20)+υ(CN7)(8)+$\rho(NO_2)$(5)
1577	1527	1562	1520	$\upsilon(NO_2)$(74)+R2[υ(C11C12)](9)
1526	1477	1492	1489	R2[υ(CC)(41)+δ_{ring}(13)+υ(CN)(5)]+υ(CC)(12)+υ(CN7)(5)
1484	1437		1435	R1[$\delta(CH_2)$](92)
1425	1379	1428	1404	R2[υ(CC)(23)+υ(OC)(31)+δ_{in}(CH15)](15)+δ_{in}(CC17)(5)]+ρ(CH)(6)
1403	1358	1378	1381	ρ(CH)(12)+R1[υ(C19N8)(11)+ω(CH_2)(8)+υ(NN)(6)]+R2[υ(C11C12)(18)+δ_{in}(CH13)(5)]
1375	1331			R1[δ_{in}(NH)(36)+υ(CN9)](17)+ρ(CH)(7)+$\upsilon(NO_2)$(7)
1363	1319	1348	1342	ρ(CH)(22)+$\upsilon(NO_2)$(30)+R2[υ(CN)(14)+υ(C12C14)(10)+δ_{in}(CH15)(5)+δ(NO2)(9)
1346	1303	1323		R1[ω(CH_2)](21)+δ_{in}(NH)(20)+υ(C19N9)(13)+υ(C19N8)(10)]+ρ(CH)(5)
1323	1281			R1[υ(CN)(26)+υ(CC)(19)+ω(CH2)(16)+δ_{in}(C=O)(14)+δ_{ring}(6)
1287	1246	1258	1250	R2[υ(C12C14)(28)+R2υ(OC11)(10)+δ_{in}(CH13)(7)]+υ(CC)(11)+$\upsilon(NO_2)$(14)+ρ(CH)(5)
1270	1229	1247	1250	R1[υ(NN)(26)+υ(C21N)(13)]+R2[υ(OC)(18)+δ_{in}(CH15)(5)+δ'_{ring}(5)]+δ(NNC)(6)
1248	1208	1235		R2[υ(OC)(34)+δ'_{ring}(10)+υ(CN)(8)+υ(C11C12)(5)]+R1[υ(NN)(16)+υ(C21N)(5)]
1209	1170	1207	1204	R1[ω(CH2)(23)+υ(C19N8)(21)+υ(C21N)(21)+υ(CN9)(5)]
1192	1154		1173	R2[δ_{in}(CH13)(31)+δ_{in}(CH15)(21)+υ(CN)(9)+δ'_{ring}(7)+υ(OC16)(5)+υ(CC)(5)]
1191	1153	1169	1173	R1[γ(CH2)](96)
1115	1079		1111	R1[υ(CN)(54)+δ_{in}(C=O4)(10)+δ_{in}(NH)(10)+υ(C21N)(7)+υ(CC)(5)]
1038	1005	1017		R2[δ_{in}(CH15)(64)+υ(C12C14)(24)]
1014	982	1017	1018	R1[ρ(CH2)(71)+OOP(C=O5)(15)+τ(6)]
1000	968	977		R2[υ(OC)(53)+δ'_{ring}(13)+υ(CC)(8)+δ_{in}(CH15)(4)
986	955	963	964	R2(δ_{ring})(42)+υ(OC)(18)+υ(CC16)(9)+υ(CN)(8)+υ(C11C12)(5)]
921	892			ω(CH)(54)+ τ(CN)(24)+R2[OOP(CH)](11)
904	875	902	903	R2[OOP(CH)(78)+τ(12)]+ω(CH)(5)
892	864			R1[υ(CC)(54)+υ(CN9)(18)+δ_{in}(NH)(7)]
879	851	870	872	R2(δ'_{ring})(17)+δ(NNC)(17)+δ_s(CH)(14)+R1[υ(C21N)(12)+δ'_{ring}(9)+υ(NN)(8)+υ(C19N8)(7)]
830	804		825	δ(NO2)(59)+R2[δ'_{ring}(17)+δ_{ring}(7)]
811	785	809		R2[OOP(CH)](88)
786	761	791	779	R1[υ(C19N8)(22)+δ'_{ring}(8)+δ_{in}(C=O4)(5)+R2[δ'_{ring}(15)+δ_{ring}(12)]+υ(CC)(7)+δ(N

				O2)(5)
741	717	783		R1[OOP(C=O4)(70)+τ'(13)+τ(8)]
738	714	714	725	ω(CN6)(66)+R2[OOP(C16N)(15)+τ'(10)
690	668			R1[δ_{ring}(26)+υ(C21N)(16)+δ_{in}(C=O)(17)+δ'_{ring}(10)+δ_{in}(NN)(10)+υ(CC)(5)]
688	666	685	687	R2[τ'(35)+OOP(CC17)(33)+τ(24)]
616	596	622		R1[δ_{in}(C=O)(32)+δ'_{ring}(15)+δ_{ring}(11)+δ_{in}(NN)(9)]+δ(NNC)(6)
608	588	606	609	R1[OOP(C=O5)(40)+OOP(NH)(38)+τ(12)+ρ(CH_2)(7)]
602	583		602	R1[δ'_{ring}(25)+δ_{ring}(19)+υ(C19N9)(10)]+υ(CC)(5)
594	575	585		R2[τ(53)+τ'(24)+OOP(C16N)(17)]
554	536			R1[OOP(NH)(54)+OOP(C=O5)(26)+ρ(CH_2)(10)+γ(CH_2)(5)]
553	535	551	548	ρ(NO2)(43)+R2[δ_{in}(C16N)(20)+δ_{in}(CC17)(10)+υ(CC16)(5)]+R1[δ_{in}(C=O)](8)
463	448	467	463	δ(NNC)(17)+ρ(NO_2)(12)+R2[δ_{in}(CC17)(15)+υ(CN)(11)+δ_{ring}(6)]+δ_s(CH)(6)+R1[δ_{in}(NN)(5)+δ_{in}(C=O)(9)]
441	427	438	440	R2[υ(CN)(19)+δ_{in}(CC17)(7)+δ'_{ring}(5)]+R1[δ_{in}(C=O5)(12)+δ_{in}(C=O4)(7)+υ(C19N9)(5)]+δ(NO_2)(8)+δ_s(CH)(6)
400	387	399	409	R1[δ_{in}(C=O)(43)+υ(C19N9)(6)+υ(CC)(6)+υ(C21N)(5)]+R2[υ(CN)(11)+δ_{ring}(5)]
378	366	386		τ(CN)(28)+R2[τ'(17)+τ(13)+OOP(CC17)(10)+OOP(C16N)(8)]+ω(CH)(9)+R1[OOP(NN)](6)
298	289		-	R1[τ(NN)(41)+OOP(NN)(20)+τ'(9)]+R2[τ(CC)](12)+τ(CN)(8)
293	283	295	-	R1[δ_{in}(NN)(18)+δ_{in}(C=O4)(17)+υ(C19N8)(6)]+R2[δ_{in}(C16N)(13)+δ_{in}(CC17)(12)]+ρ(NO_2)(7)+υ(CC)(6)
222	214	223	-	R2[δ_{in}(C16N)(33)+δ_{ring}(5)+ρ(NO_2)(17)+δ_s(CH)(12)+υ(CC)(6)
194	188	202	-	R2[OOP(C16N)(56)+OOP(CC17)(6)]+R1[τ(NN)](13)+τ(CN)(7)
178	173	181	-	R1[τ'(77)+OOP(NN)(16)]
142	137	-	-	R1[τ(54)+OOP(NH)(36)]
136	132	-	-	R1[δ_{in}(NN)](30)+δ(NNC)(21)+R2[δ_{in}(C16N)(18)+δ_{in}(CC17)(13)]
121	117	-	-	R1[τ(34)+OOP(NH)(21)+OOP(NN)(5)]+R2[OOP(CC17)(10)+τ(CN)(10)+OOP(C16N)(9)]
75	73	-	-	R2[τ(CN)](42)+R1[OOP(NN)(31)+τ'(9)]
50	49	-	-	δ_s(CH)(36)+R2[δ_{in}(CC17)(29)+δ_{in}(C16N)(5)]+δ(NNC)(17)+R1[δ_{in}(NN)](6)
44	43	-	-	R1[OOP(NN)(30)+τ'(11)]+R2[τ(CN)(20)+τ(CC)(18)+OOP(CC17)(8)]
24	23	-	-	R1[OOP(NN)(37)+τ(NN)(19)+τ(5)]+R2[τ(CC)](20)+τ(CN)(7)

Table S3 Theoretical and experimental vibrational wavenumbers (cm^{-1}) of urea with PED.

Unscaled DFT	Scaled DFT	Raman	IR	Assignment
3690	3571	-	3468	ν_a($N2H_2$)(96)
3688	3570	-	3468	ν_a($N5H_2$)(96)
3579	3464	-	3340	ν_s($N2H_2$)(58)+ν_s($N5H_2$)(41)
3573	3459	-	3340	ν_s($N5H_2$)(59)+ν_s($N2H_2$)(41)
1786	1729	1649	1690	ν(C=O)(68)+ν(CN)(12)+ δ(NCN)(6)
1633	1581	1624	1626	δ(NH_2)(89)+ν(CN)(10)
1632	1580	1542	1588	δ(NH_2)(90)+ν(C=O)(7)
1404	1359	-	1464	ν(CN2)(58)+ρ(OCN)(15)+ρ(CN5)(8)+ρ(CN2)(8)+δ(NCN)(5)
1177	1139	1176	1153	ρ(NH_2)(77)+ν(C=O)(17)
1040	1006	1011	1051	ρ(NH_2)(68)+ν_a(CN_2)(28)
950	920	-	1000	ν(CN)(91)
777	752	-	786	ω(C=O)(85)
579	561	562	573	ρ(OCN)(58)+δ(NCN)(19)+ρ(CN2)(5)+ρ(CN5)(5)
545	527	546	560	ω(CN5)(49)+ω(CN2)(32)+ν(CN5)(5)
538	520			ω(CN2)(31)+τ(CN2)(15)+τ(CN5)(11)+ω(CN5)(10)+ρ(OCN)(8)+ω(NCN)(7)+ν(CN2)(5)
477	462	-	-	δ(NCN)(59)+ρ(CN5)(20)+ρ(CN2)(9)+ρ(CN5)(9)

445	431	-	-	ω(CN2)(26)+ρ(OCN)(24)+τ(CN5)(18)+τ(CN2)(17)+ν(CN2)(6)+ν(CN5)(6)
364	352	-	-	τ(CN2)(39)+τ(CN5)(39)+ω(CN2)(6)+ω(CN5)(6)+δ(NCN)(5)

Table S4 Theoretical and experimental vibrational wavenumbers (cm^{-1}) of NF-urea with PED.

Frequency NF-urea (monomer)		Experimental							Cal. Scaled Freq. (cm^{-1})	Simplified description of modes of dimer
Calculated		Experimental		NF		urea		Assignment		
Unscaled DFT	Scaled DFT	Raman	IR	Raman	IR	Raman	IR		Monomer + 3urea	
3690	3571	-	3485	-	3503	-	3468	$\upsilon_a(N25H_2)(98)$	3606,3588,3576,3558	NH_2asym stretch
3684	3566	-		-		-		$\upsilon_a(N28H_2)(99)$	3545,3507,3497,3480	NH_2asym stretch
3627	3511	-	3466	-	3287	-	-	R1[υ(NH)](99)	2862	Ring1 NH stretch
3572	3457	-		-	-	-	3340	$\upsilon_s(N25H_2)(89)+\upsilon_s(N28H_2)(11)$	3486,3476,3465,	NH_2sym stretch
3558	3444	-	3364	-	-	-		$\upsilon_s(N28H_2)(88)+\upsilon_s(N25H_2)(11)$	3411,3374,3308,3264	NH_2sym stretch
3279	3174	3156	3157	-	3148	-	-	R2[υ(CH)](99)	3172	Ring2 CH stretch
3250	3146	3122	3121	-	3109	-	-	R2[υ(CH)](99)	3122	Ring2 CH stretch
3104	3004	3026	3024	-	3017	-	-	υ(CH)(99)	3003	CH stretch
3081	2982	2947	2947	-	2947	-	-	$R1[\upsilon_a(CH_2)](100)$	2983	Ring1 CH_2asym stretch
3038	2940	2912	2912	-	2916	-	-	$R1[\upsilon_s(CH_2)](99)$	2940	Ring1 CH_2 sym stretch
1860	1800	1781	1782	1979	1830	-	-	$R1[\upsilon_s(C=O)(80)+\delta'_{ring}(8)]$	1781	Ring1 C=O stretch
1827	1768		1732		1780	-	-	$R1[\upsilon_a(C=O)(75)+\delta_{ring}(5)]$	1746	Ring1 C=O stretch
1765	1719		1732	-	-	1649	1690	υ(C=O)(64)+υ(C31N)(14)+ρ(C=O)(6)	1692	C=O stretch
1662	1609		1620	1608	1605	-	-	υ(CN7)(54)+υ(CC)(15)+ρ(CH)(15)+R2[υ(C11C12)](6)	1602	CN stretch
1642	1589	1611	1620	-	-	1624	1626	$\delta(NH_2)(72)+\delta$(O4HN25)(17)	1668,1650,1618,	NH_2 deformation
1636	1583		1593	-	-	1542	1588	$\delta(NH_2)(85)+\upsilon$(C31N)(10)	1614,1602,1580	NH_2 deformation
1603	1552	1571	1570	1601	1566	-	-	$R2[\upsilon(CC)(45)+\delta_{in}(CH13)(6)+\delta_{in}(C16N)(5)]+\upsilon_a(NO_2)(18)+\upsilon$(CN7)(8)+$\rho(NO_2)(5)$	1549	Ring2 CC stretch
1579	1528	1571	1549	1562	1520	-	-	$\upsilon_a(NO_2)(72)$+R2[υ(C11C12)](9)+$\rho(NO_2)(5)$	1520	NO_2 stretch
1527	1478	1499	1524	1492	1489	-	-	$R2[\upsilon(CC16)(29)+\upsilon(C11C12)(12)+\delta_{ring}(13)+\upsilon(CN)(5)]+\upsilon(CC)(12)+\upsilon(CN7)(5)$	1478	Ring2 CC stretch
1484	1436	1437	1439		1435	-	-	$R1[\delta(CH_2)](90)$	1434	Ring1 CH_2 sym stretch
1425	1379	1397	1402	1428	1404	-	-	$R2[\upsilon(CC)(21)+\upsilon(OC)(26)+\delta_{in}(CH)(14)+\delta_{in}(C16N)(5)+\delta_{in}(CC17)(7)]$	1436,1376	Ring2 CC stretch
1411	1366	1375	1381	-	-		1464	$\upsilon(C31N)(44)+\delta_s(C=O24)(12)+\rho(NH_2)(14)$	1450,1429,1410,1401	CN stretch
1406	1361	1349	1358	1378	1381	-	-	$R1[\upsilon(C19N8)(11)+\omega(CH_2)(7)]+\rho(CH)(10)+R2[\upsilon(C12C14)(8)+\delta_{in}(CH13)(5)]+\upsilon(NN)(5)$	1356	Ring1 CN stretch
1374	1330	1338	1342			-	-	$R1[\delta_{in}(NH)(33)+\upsilon(CN9)(13)]+\rho(CH)(6)+\upsilon_S(NO_2)(12)$	1436	Ring1 NH in plane bend
1364	1320	1334		1348	1342	-	-	$\rho(CH)(25)+\upsilon_s(NO_2)(27)$+R2[υ(CN)(12)+υ(C12C14)(5)]+$\delta(NO_2)(9)$	1316	NO_2 stretch
1352	1309	1313	1313			-	-	$R1[\delta_{in}(NH)(25)+\upsilon(C19N9)(25)+\omega(CH_2)(12)]+\upsilon$	1316	Ring1 NH in

								$(NO_2)(8)$		plane bend
1322	1280	1260	1261	1323		-	-	R1[$\omega(CH_2)(22)+\upsilon(CC)(18)+\upsilon(CN9)(23)+\delta_{in}(C=O)(11)+\delta_{ring}(7)]+\rho(CH)(5)$	1283	Ring1 CH_2 wagging
1287	1246	1250	1248	1258		-	-	R2[$\upsilon(C12C14)(28)+\upsilon(OC11)(11)+\delta_{in}(CH13)(6)]+\upsilon(CC)(12)+\upsilon(NO_2)(13)+\rho(CH)(6)$	1242	Ring2 NN stretch
1272	1231	1237	1236	1247	1250	-	-	R1[$\upsilon(NN)(25)+\upsilon(C21N)(13)]$+R2[$\upsilon(OC16)(11)+\upsilon(OC11)(7)]+\delta_s(NNC)(7)+\delta_s(CH18)(6)$	1236,1209	Ring1 NN stretch
1248	1208	1207	1209	1207	1204	-	-	R2[$\upsilon(OC)(34)+\delta'_{ring}(10)+\upsilon(CN)(7)]$+R1[$\upsilon(NN)(16)+\upsilon(C21N)(6)]$	1176	Ring2 OC stretch
1213	1174	1181	1178	1169	1173	-	-	R1[$\omega(CH_2)(24)+\upsilon(CN8)(39)+\upsilon(CN9)(7)]$	1152	Ring1 CH_2 wagging
1193	1155		1134			-	-	R2[$\delta_{in}(CH)(47)+\upsilon(CN)(10)+\delta'_{ring}(7)+\upsilon(OC16)(6)]+\upsilon(CC)(5)$+R1[$\gamma(CH_2)](5)$	1157	Ring2CH in plane bend
1192	1154					-	-	R1[$\gamma(CH_2)](91)$	1152	Ring1 CH_2 twisting
1186	1148			-	-	1176	1153	$\rho(NH_2)(67)+\upsilon(C=O)(15)+\delta(O4HN25)(11)$	1169,1136,1145	NH_2 rocking
1122	1086	1041	1055	1123	1111	-	-	R1[$\upsilon(CN9)(52)+\delta_{in}(NH)(10)+\delta_{in}(C=O4)(9)+\upsilon(C21N)(6)+\upsilon(CC)(6)]$	1126	Ring1 CN stretch
1054	1020		1034	-	-	1011	1051	$\rho(NH_2)(61)+\upsilon(C31N)(22)+\delta(O4HN25)(13)$	1075,1037,1029,1018	NH_2 rocking
1040	1007	1007				-	-	R2[$\delta_{in}(CH)(62)+\upsilon(C12C14)(25)$	1006	Ring2 CH in plane bend
1012	980			1017	1018	-	-	R1[$\rho(CH_2)(71)+OOP(C=O5)(15)+\tau(6)]$	987	Ring1 CH_2 rocking
1002	969	991		977		-	-	R2[$\upsilon(OC)(52)+\delta'_{ring}(12)]+\upsilon(CC)(8)$	980	Ring2 OC stretch
988	956	979	978	963	964	-	-	R2[$\delta_{ring}(41)+\upsilon(OC)(17)+\upsilon(CC16)(9)+\upsilon(CN)(8)+\upsilon(C11C12)(5)]$	968	Ring2 deformation
958	928	920	920	-	-	-	1000	$\upsilon(C31N)(84)+\rho(N25H_2)(8)$	967,962,949	CN stretch
926	896				926	-	-	$\omega(CH)(54)+\tau(CN)(25)$+R2[$OOP(CH)](10)$	890,879	CH wagging
907	878	898	893	902	903	-	-	R2[$OOP(CH)](78)+\tau(12)]+\omega(CH)(5)$	955	Ring2 CH out of plane bend
889	860		893			-	-	R1[$\upsilon(CC)(53)+\upsilon(CN9)(18)+\delta_{in}(NH)(7)]$	876	Ring CC stretch
881	853	876	872, 862	870	872	-	-	$\delta_s(CH)(19)+\delta_s(NNC)(18)$+R2($\delta'_{ring}$)(14)+R1[$\upsilon(CN8)(18)+\delta'_{ring}(8)+\upsilon(NN)(8)]$	847	CH symmetric deformation
832	805		816		825	-	-	$\delta(NO_2)(59)$+R2[$\delta'_{ring}(17)+\delta_{ring}(7)]+\upsilon(NO_2)(8)$	804	NO_2 deformation
816	790	817	816	809		-	-	R2[$OOP(CH)](87)$	790	Ring1 CN stretch
791	765	791	785	783	779	-	-	R1[$\upsilon(C19N8)(19)+\delta'_{ring}(8)+\delta_{in}(C=O4)(5)]$+R2[$\delta'_{ring}(15)+\delta_{ring}(12)]+\upsilon(CC)(6)+\delta_s(CH)(6)+\delta(NO_2)(5)$	769	Ring1 CN stretch
779	754			-	-	-	786	$\omega(C=O24)(89)$	786,756,751	C=O wagging
744	720	748	748			-	-	R1[$OOP(C=O4)(71)+\tau'(14)+\tau(8)]$	761	Ring1 C=O out of plane bend
735	711	737	737	714	725	-	-	$\omega(CN6)(67)$+R2[$OOP(C16N)(16)+\tau'(11)]$	714	CN wagging
692	670	690	689			-	-	R1[$\delta_{ring}(25)+\upsilon(C21N)(15)+\delta'_{ring}(10)+\delta_{in}(C=O4)(10)+\delta_{in}(NN)(9)+\upsilon(CC)(5)+\delta_{in}(C=O5)(5)]+\delta_s(CH)(5)$	734	Ring1 deformation
685	663	665	669	685	687	-	-	R2[$\tau'(35)+OOP(CC17)(34)+\tau(23)]+\tau(CN)(4)$	665	Ring2 torsion
619	599	625	617	622		-	-	R1[$\delta_{in}(C=O)(30)+\delta'_{ring}(16)+\delta_{in}(NN)(10)+\delta_{ring}(7)]+\delta_s(NNC)(7)$	669	Ring1 C=O in plane bend
609	590	609	609					$\tau(C31N)(37)+\delta_s(C=O24)(16)+\delta(O4HN25)(14)+\delta(N25HN7)(6)+\rho(C=O24)(5)$	640	CN torsion
606	587			606	609	-	-	R1[$OOP(C=O5)(24)+OOP(NH)(23)+\delta_{ring}(8)+\tau(7)+\delta'_{ring})(7)]$	611	Ring1 out of plane bend

604	585				602	-	-	R1[OOP(C=O5)(23)+OOP(NH)(22)+δ'$_{ring}$(10)+δ$_{ring}$(8)+τ(7)]	595	Ring1 out of plane bend
593	573	584	596	585		-	-	R2[τ(52)+τ'(24)+OOP(C16N)(17)]	574	Ring2 torsion
562	544	578	561	-	-	562	573	δ$_s$(C=O24)(29)+δ(O4HN25)(18)+ρ(C=O24)(11)+τ(N25C)(11)+ρ(NH$_2$)(12)+δ(O3HN25)(5)	587	C=O symmetric deformation
554	536		555	570		-	-	R1[OOP(NH)(33)+OOP(C=O5)(18)+ρ(CH$_2$)(7)]+ρ(NO$_2$)(12)+R2[δ$_{in}$(C16N)](6)	572,571	Ring1 NH out of plane bend
553	536	553	544	551	548	-	-	ρ(NO$_2$)(29)+R2[δ$_{in}$(C16N)(15)+δ$_{in}$(CC17)(8)]+R1[OOP(NH)(13)+OOP(C=O5)(7)]	537	NO$_2$ rocking
535	518		525	-	-	546	560	ω(CN28)(73)+υ(CN28)(12)+R1[OOP(NH)](5)	583,582,575	CN wagging
500	484	470	507	-	-			ρ(C=O)(36)+δ(O4HN25)(19)+δ$_s$(C=O)(15)+τ(N28C)(7)+ρ(N25H$_2$)(6)	532,530	C=O rocking
483	468		480	-	-			ω(CN25)(26)+τ(N28C)(25)+δ(N25HN7)(19)+ρ(C=O)(9)	518,510,489	CN wagging
464	450	470	459	467	463	-	-	δ$_s$(NNC)(17)+R2[δ$_{in}$(CC17)(16)+υ(CN)(9)+δ$_{ring}$(5)]+ρ(NO$_2$)(11)+δ$_s$(CH)(7)+R1[δ$_{in}$(NN)](5)	450,288	NNC deformation
442	428		444	438	440	-	-	R2[υ(CN)(17)+δ$_{in}$(CC17)(7)+δ'$_{ring}$(5)]+R1[δ$_{in}$(C=O)(18)]+δ$_s$(CH)(8)+δ(NO$_2$)(8)	472	Ring1 C=O in plane bend
429	415	409	418	-	-			δ(O4HN25)(34)+δ(N25HN7)(33)+τ(N25C)(11)+τ(N28C)(8)+ω(CN25)(8)	398,388	OHN deformation
402	389	409	409	399	409	-	-	R1[δ$_{in}$(C=O)(41)+υ(CC)(6)+υ(CN9)(10)+υ(C21N)(5)]+R2[υ(CN)(11)+δ$_{ring}$(5)]	349	Ring1 C=O in plane bend
379	366	386		386		-	-	τ(CN)(29)+R2[τ'(16)+τ(13)+OOP(CC17)(9)+OOP(C16N)(8)]+ω(CH)(8)+R1[OOP(NN)](7)	368,223	CN torsion
299	290	305	-		-	-	-	R1[τ(NN)(33)+OOP(NN)(16)+τ'(7)]+R2[τ(CC)](14)+τ(CN)(7)+δ(N8NH27)(5)	301,205	Ring1 NN torsion
295	285	296	-	295	-	-	-	R1[δ$_{in}$(NN)(12)+δ$_{in}$(C=O4)(10)+τ(NN)(8)]+R2[δ$_{in}$(CC17)(10)+δ$_{in}$(C16N)(10)]+δ(O4HN25)(5)+ρ(NO$_2$)(5)	191	Ring1 NN in plane bend
224	217	212	-	223	-	-	-	R2[δ$_{in}$(C16N)](32)+ρ(NO$_2$)(15)+δ$_s$(CH)(14)+υ(CC)(5)+δ(N6OH26)(5)	186,169	Ring2 CN in plane bend
193	187	196	-	202	-	-	-	R2[OOP(C16N)(52)+OOP(CC17)(5)]+R1[τ(NN)](14)+τ(CN)(6)	162,159	Ring2 CN out of plane bend
189	183		-	181	-	-	-	R1[τ'(71)+OOP(NN)(15)+OOP(NH)(5)]	145,140	Ring1 torsion
150	145	156	-	-	-	-	-	R1[τ(50)+OOP(NH)(29)+OOP(NN)(6)+τ'(5)]	137,129	Ring1 torsion
139	135	149	-	-	-	-	-	R1[δ$_{in}$(NN)](25)+δ$_s$(NNC)(19)+R2[δ$_{in}$(C16N)(15)+δ$_{in}$(CC17)(14)]+δ(N6OH26)(5)	140,137	Ring1 NN in plane bend
124	120	119	-	-	-	-	-	R1[τ(18)+OOP(NN)(6)+OOP(NH)(10)]+R2[τ(CN)(16)+OOP(CC17)(12)+OOP(C16N)(10)+τ(CC)(6)]	108,100	Ring1 torsion
97	94	109	-	-	-	-	-	δ(O4HN25)(41)+R1[τ(15)+OOP(NH)(10)]+δ(N8NH27)(5)+δ(O3HN25)(5)	94,86	OHN deformation
80	77		-	-	-	-	-	R2[τ(CN)](35)+R1[OOP(NN)(20)+τ(10)+δ(N6OH26)(16)	83,81	Ring2 CN torsion
72	69	70	-	-	-	-	-	δ(O4HN25)(40)+ω(CN25)(10)+δ(N25HN7)(9)+ω(CN28)(7)+δ(N6OH26)(7)+τ(N28C)(6)+δ(COH30)(5)	76,73	OHN deformation
65	63		-	-	-	-	-	δ(N6OH26)(29)+δ(O4HN25)(17)+ω(CN25)(14)+δ(COH30)(9)+δ(O3HN25)(5)	73,64	NOH deformation
61	59	-	-	-	-	-	-	δ$_s$(CH)(14)+δ(N8NH27)(14)+δ(N25HN7)(11)+δ(O4HN25)(10)+δ(N6OH26)(9)+R2[δ$_{in}$(CC17)](9)+δ$_s$(NNC)(6)+δ(O3HN25)(5)	60,56	CH deformation
51	50	-	-	-	-	-	-	δ(O3HN25)(30)+R1[OOP(NN)](13)+R2[τ(CC)](10)+δ(N25HN7)(10)+δ(O4HN25)(9)	49,44	OHN deformation

42	41	-	-	-	-	-	-	δ(O4HN25)(45)+δ(N8NH27)(29)+δ(N25HN7)(15)	38,36	OHN deformation
33	32	-	-	-	-	-	-	δ(O3HN25)(34)+R1[OOP(NN)](17)+δ(O4HN25)(13)+R2[τ(CN)](7)+ω(CN25)(5)	31,24	OHN deformation
22	21	-	-	-	-	-	-	δ(N8NH27)(21)+δ(O4HN25)(16)+R2[τ(CC)](16)+R1[τ(NN)(12)+OOP(NN)](11)]+δ(N25HN7)(7)	22,18	NNH deformation
13	13	-	-	-	-	-	-	δ(N25HN7)(39)+δ(O4HN25)(21)+δ(COH30)(19)+δ(N6OH26)(7)+δ(N8NH27)(7)	15,12	NHN deformation

Table S5 Geometrical parameters (bond length) and topological parameters for hydrogen bonds of interacting atoms of cocrystal (monomer + 3urea): electron density (ρ_{BCP}), Laplacian of electron density ($\nabla^2\rho_{BCP}$), electron kinetic energy density (G_{BCP}), electron potential energy density (V_{BCP}), total electron energy density (H_{BCP}) at bond critical point (BCP) and estimated interaction energy (E_{int}).

Interactions	Bond length	ρ_{BCP}	$\nabla^2\rho_{BCP}$	G_{BCP}	V_{BCP}	H_{BCP}	E_{int}
O32···H10	1.67082	0.04761	0.13818	−0.00525	−0.04505	−0.05030	−31.5637
O24···H53	1.79262	0.03602	0.11629	−0.00046	−0.02999	−0.03045	−19.1077
O32···H45	1.93082	0.02663	0.09375	−0.00173	−0.01997	−0.02170	−13.6170
O40···H37	1.91980	0.02642	0.09289	−0.00189	−0.01944	−0.02133	−13.3848
O48···H35	2.04629	0.01896	0.07606	−0.00278	−0.01345	−0.01623	−10.1845
O4···H30	2.03885	0.01842	0.07363	−0.00292	−0.01256	−0.01548	−9.7138
O48···H29	2.08743	0.01887	0.06508	−0.00194	−0.01238	−0.01432	−8.9859
O48···H38	2.20677	0.01442	0.05183	−0.00186	−0.00924	−0.01110	−6.9653
O5···H46	2.45626	0.00889	0.02948	−0.00099	−0.00539	−0.00638	−4.0035
O4···H34	2.57557	0.00770	0.02505	−0.00079	−0.00469	−0.00548	−3.4387
O3···H26	2.64432	0.00571	0.02327	−0.00099	−0.00384	−0.00483	−3.0308
O1···H27	2.94638	0.00262	0.01103	−0.00060	−0.00156	−0.00216	−1.3554
N7···H27	3.35510	0.00149	0.00555	−0.00035	−0.00069	−0.00104	−0.6526

Bond length (in Å); ρ_{BCP}, $\nabla^2\rho_{BCP}$, G_{BCP}, V_{BCP}, H_{BCP} (in a.u.); E_{int} (in kcal mol^{-1}).

Table S6 Geometrical parameters for intermolecular hydrogen bond in NF-urea (monomer + 3urea): bond length (Å), bond angle (◦) and sum of van der Waals radii of interacting atoms (Å).

D-H···A	D-H	H···A	D-H···A	(r_H+ r_A) (Å)
N9-H10···O32	1.04860	1.67082	166.87133	2.72
N52-H53···O24	1.03213	1.79262	176.58883	2.72
N44-H45···O32	1.02046	1.93082	166.52778	2.72
N36-H37···O40	1.02201	1.91980	174.15750	2.72
N33-H35···O48	1.01346	2.04629	150.19926	2.72
N28-H30···O4	1.01159	2.03885	167.18286	2.72
N28-H29···O48	1.01492	2.08743	170.63755	2.72
N36-H38···O48	1.01187	2.20677	144.85794	2.72
N44-H46···O5	1.01045	2.45626	134.10930	2.72
N33-H34···O4	1.00811	2.57557	128.25881	2.72
N25-H26···O3	1.00624	2.64432	113.75347	2.72

Table S7 Geometrical parameters (bond length) and topological parameters for hydrogen bonds of interacting atoms of NF-urea (monomer): electron density (ρ_{BCP}), Laplacian of electron density ($\nabla^2\rho_{BCP}$), electron kinetic energy density (G_{BCP}), electron potential energy density (V_{BCP}), total electron energy density (H_{BCP}) at bond critical point (BCP) and estimated interaction energy (E_{int}).

Interactions	Bond length	ρ_{BCP}	$\nabla^2\rho_{BCP}$	G_{BCP}	V_{BCP}	H_{BCP}	E_{int}
O4···H30	2.21754	0.01272	0.04853	−0.00203	−0.00808	−0.01011	−4.7754
O4···H27	2.67752	0.00549	0.01959	−0.00080	−0.00330	−0.00410	−4.6513
N7···H27	2.66864	0.00655	0.01978	−0.00084	−0.00327	−0.00411	−3.8609

O1···N25	3.36319	0.00406	0.01636	−0.00076	−0.00257	−0.00333	−1.4859
O3···H26	2.38129	0.00878	0.03161	−0.00135	−0.00521	−0.00656	−1.2482

Table S8 Second order perturbation theory analysis of Fock matrix in NBO basis for intramolecular interactions for monomer unit 1 and 2 within NF-urea (monomer + 3urea).

Donor NBO (i)	ED(i)/e	Acceptor NBO (j)	ED(j)/e	E(2)[a] kcal mol^{-1}	E(j)−E(i)[b]	F(i,j)[c]
within unit 1						
πO3-N6	1.98264	n(3)O2	1.46522	11.55	0.18	0.077
		π*O3-N6	0.66610	8.08	0.31	0.055
		π*C14-C16	0.31455	5.35	0.45	0.048
πN7-C17	1.91207	π*C11-C12	0.32461	12.01	0.35	0.062
πC11-C12	1.74905	π*N7-C17	0.24494	14.21	0.34	0.062
		π*C14-C16	0.31455	18.82	0.29	0.067
σC12-C14	1.96704	σ*N6-C16	0.10014	7.93	1.00	0.081
		σ*C11-C17	0.03050	5.56	1.16	0.072
πC14-C16	1.77379	π*O3-N6	0.66610	24.76	0.17	0.065
		π*C11-C12	0.32461	14.31	0.30	0.060
σC17-H18	1.97829	σ*O1-C11	0.02859	5.77	0.90	0.064
n(2)O1	1.70147	π*C11-C12	0.32461	29.14	0.36	0.092
		π*C14-C16	0.31455	28.04	0.36	0.090
n(2)O2	1.89341	σ*O3-N6	0.05638	18.70	0.72	0.105
		σ*N6-C16	0.10014	11.16	0.59	0.073
n(3)O2	1.46522	π*O3-N6	0.66610	161.19	0.14	0.137
n(2)O3	1.89491	σ*O2-N6	0.05533	18.54	0.72	0.104
		σ*N6-C16	0.10014	12.63	0.59	0.077
n(2)O4	1.83839	σ*N8-C19	0.10051	28.64	0.64	0.123
		σ*N9-C19	0.07473	23.94	0.71	0.119
n(2)O5	1.85256	σ*N9-C20	0.07810	25.50	0.71	0.122
		σ*C20-C21	0.07419	22.88	0.60	0.107
n(1)N7	1.91282	σ*N8-C21	0.04131	12.13	0.70	0.083
		σ*C17-H18	0.03128	10.37	0.76	0.080
n(1)N8	1.64034	π*O4-C19	0.33698	49.90	0.29	0.108
		π*N7-C17	0.24494	30.87	0.34	0.094
		σ*C21-H23	0.01813	5.66	0.66	0.060
n(1)N9	1.60179	π*O4-C19	0.33698	56.80	0.27	0.112
		π*O5-C20	0.25278	58.25	0.27	0.116
π*O3-N6	0.66610	π*C14-C16	0.31455	19.20	0.14	0.066
π*C11-C12	0.32461	π*N7-C17	0.24494	29.18	0.05	0.063
within unit 2						
n(2)O24	1.85765	σ*N25-C31	0.05874	21.93	0.73	0.115
		σ*N28-C31	0.05714	16.17	0.74	0.100
n(1)N25	1.78458	σ*O24-C31	0.30077	21.04	0.46	0.089
		π*O24-C31	0.14940	9.08	0.67	0.071
n(1)N28	1.77923	σ*O24-C31	0.30077	27.30	0.46	0.102
σ*O24-C31	0.30077	π*O24-C31	0.14940	91.70	0.21	0.263
π*O24-C31	0.14940	σ*N25-H26	0.00540	7.60	0.03	0.052
		σ*N28-H30	0.01859	5.74	0.05	0.050

[a]E(2) means energy of hyper conjugative interaction (stabilization energy). [b]Energy difference between donor (i) and acceptor (j) NBO orbitals.

[c]F(i,j) is the Fock matrix element between i and j NBO orbitals.

Table S9 Second order perturbation theory analysis of Fock matrix in NBO basis for the intermolecular interactions for NF-urea (monomer + 3urea).

Donor NBO (i)	ED(i)/e	Acceptor NBO (j)	ED(j)/e	E(2)[a] kcal mol^{-1}	E(j)−E(i)[b]	F(i,j)[c]
From unit 1 to unit 2						
n(1)O4	1.97316	σ*N28-H30	0.01859	2.72	1.19	0.051
From unit 1 to unit 3						
σN9-H10	1.98125	π*O32-C39	0.45779	0.67	0.71	0.022
From unit 1 to unit 4						

π*N7-C17	0.24494	π*O40-C47	0.36294	1.52	0.04	0.012
From unit 1 to unit 5						
π*N7-C17	0.24494	σ*N49-H51	0.00818	7.49	3.02	0.377
From unit 2 to unit 5						
n(1)O24	1.96539	σ*N52-H53	0.04783	5.80	1.15	0.073
n(2)O24	1.85765	σ*N52-H53	0.04783	13.44	0.74	0.091
π*O24-C31	0.14940	σ*N52-H53	0.04783	4.11	0.07	0.048
From unit 3 to unit 1						
πO32-C39	1.97310	σ*N9-H10	0.07402	7.15	0.76	0.067
n(1)O32	1.94169	σ*N9-H10	0.07402	13.60	1.08	0.109
n(2)O32	1.87746	σ*N9-H10	0.07402	5.39	0.65	0.053
π*O32-C39	0.45779	σ*N9-H10	0.07402	3.01	0.36	0.057
From unit 3 to unit 4						
n(1)O32	1.94169	σ*N44-H45	0.02929	4.79	1.16	0.067
n(2)O32	1.87746	σ*N44-H45	0.02929	5.47	0.73	0.058
From unit 4 to unit 3						
n(1)O40	1.96954	σ*N36-H37	0.03213	3.95	1.14	0.060
n(2)O40	1.86134	σ*N36-H37	0.03213	7.86	0.72	0.069
From unit 4 to unit 5						
π*O40-C47	0.36294	σ*N49-H51	0.00818	0.57	2.98	0.086
From unit 5 to unit 1						
σO48-C55	1.99224	σ*N9-C19	0.07473	2.44	1.43	0.054
		σ*C12-H13	0.01167	5.73	1.50	0.083
		σ*C14-H15	0.01081	2.18	1.44	0.050
σN49-H51	1.98771	π*N7-C17	0.24494	2.12	0.71	0.037
σN49-C55	1.99323	π*N7-C17	0.24494	2.80	0.85	0.046
		σ*C14-C16	0.01834	2.49	1.39	0.053
σN52-H53	1.98592	σ*C12-H13	0.01167	2.35	1.14	0.046
σN52-C55	1.99288	π*N7-C17	0.24494	4.53	0.87	0.060
		σ*C12-H13	0.01167	4.61	1.33	0.070
		σ*C12-C14	0.00890	2.61	1.38	0.054
n(1)O48	1.96520	σ*C12-H13	0.01167	3.18	1.20	0.055
n(2)O48	1.87387	π*N7-C17	0.24494	8.07	0.29	0.045
		σ*C12-H13	0.01167	2.97	0.76	0.044
		σ*C12-C14	0.00890	2.46	0.80	0.041
From unit 5 to unit 2						
n(1)O48	1.96520	σ*N28-H29	0.02088	2.37	1.17	0.047
n(2)O48	1.87387	σ*N28-H29	0.02088	3.96	0.73	0.049
From unit 5 to unit 3						
n(1)O48	1.96520	σ*N33-H35	0.01786	3.08	1.16	0.054
From unit 5 to unit 4						
σO48-C55	1.99129	σ*N44-H46	0.01071	3.77	1.47	0.067
n(1)O48	1.96520	σ*N44-H46	0.01071	2.24	1.17	0.046

Table S10 Selected Lewis orbitals (occupied bond orbital) with percentage ED over bonded atoms (ED_X, ED_Y in %), hybrid NBOs with s and p character in % for NF-urea (monomer).

Bond (X-Y) (ED_{X-Y})	ED_X (%) ED_Y (%)	Hybrid NBOs	s (%)	p (%)
σ(O1-C11)	68.91	$0.8301(sp^{2.13})_O$ +	31.94	67.98
(1.98555)	31.09	$0.5576(sp^{3.35})_C$	22.93	76.82
σ(O1-C16)	68.37	$0.8269(sp^{2.23})_O$ +	30.98	68.94
(1.98847)	31.63	$0.5624(sp^{2.87})_C$	25.78	73.95
σ(O2-N6)	50.27	$0.7090(sp^{3.15})_O$+	24.08	75.78
(1.99540)	49.73	$0.7052(sp^{2.07})_N$	32.54	67.33
σ(O3-N6)	50.35	$0.7096(sp^{3.10})_O$ +	24.36	75.50
(1.99624)	49.65	$0.7046(sp^{2.06})_N$	32.59	67.29
σ(O4-C19)	63.86	$0.7991(sp^{1.47})_O$ +	40.42	59.45
(1.99349)	36.14	$0.6012(sp^{1.71})_C$	36.81	63.06
σ(O5-C20)	64.24	$0.8015(sp^{1.42})_O$ +	41.30	58.57
(1.99583)	35.76	$0.5980(sp^{1.81})_C$	35.53	64..33
σ(N6-C16)	61.81	$0.7862(sp^{1.89})_N$ +	34.60	65.35

(1.98989)	38.19	$0.6180(sp^{2.40})_C$	29.42	70.47
σ(N7-N8)	45.81	$0.6769(sp^{2.97})_N$ +	25.18	74.68
(1.98790)	54.19	$0.73361(sp^{2.11})_N$	32.18	67.76
σ(N7-C17)	59.57	$0.7718(sp^{1.40})_N$ +	41.70	58.21
(1.98298)	40.43	$0.6358(sp^{2.03})_C$	33.02	66.89
σ(N8-C19)	63.26	$0.7953(sp^{1.97})_N$ +	33.71	66.24
(1.98342)	36.74	$0.6062(sp^{2.16})_C$	31.61	68.27
σ(N8-C21)	62.81	$0.7925(sp^{1.94})_N$ +	34.05	65.92
(1.98801)	37.19	$0.6098(sp^{3.51})_C$	22.16	77.70
σ(N9-H10)	72.04	$0.8488(sp^{2.24})_N$ +	30.88	69.08
(1.98732)	27.96	$0.5287(sp^{0.00})_H$	99.93	0.07
σ(N9-C19)	62.42	$0.7901(sp^{1.98})_N$ +	33.53	66.41
(1.98411)	37.58	$0.6130(sp^{2.18})_C$	31.36	68.51
σ(N9-C20)	62.90	$0.7931(sp^{1.82})_N$ +	35.46	64.49
(1.98846)	37.10	$0.6091(sp^{2.29})_C$	30.39	69.50
σ(O24-C31)	64.22	$0.8014(sp^{1.67})_O$ +	37.36	62.52
(1.99368)	35.78	$0.5981(sp^{2.01})_C$	33.18	66.66
σ(N25-H26)	70.55	$0.8400(sp^{2.40})_N$ +	29.39	70.56
(1.98799)	29.45	$0.5427(sp^{0.00})_H$	99.94	0.06
σ(N25-H27)	70.14	$0.8375(sp^{2.36})_N$ +	29.73	70.22
(1.98744)	29.86	$0.5464(sp^{0.00})_H$	99.93	0.07
σ(N25-C31)	60.79	$0.7797(sp^{1.73})_N$ +	36.61	63.33
(1.99359)	39.21	$0.6262(sp^{2.03})_C$	33.01	66.90
σ(N28-H29)	69.40	$0.8330(sp^{2.66})_N$ +	27.34	72.60
(1.98802)	30.60	$0.5532(sp^{0.00})_H$	99.94	0.06
σ(N28-H30)	69.94	$0.8363(sp^{2.46})_N$ +	28.86	71.08
(1.98682)	30.06	$0.5482(sp^{0.00})_H$	99.93	0.07
σ(N28-C31)	60.98	$0.7809(sp^{1.82})_N$ +	35.40	64.53
(1.99332)	39.02	$0.6247(sp^{2.12})_C$	32.06	67.84

Table S11 Calculated and observed ^{13}C NMR chemical shifts (δ/ppm) of NF-Urea, NF and Urea.

Atom	δ_{cal}	δ_{exp}	Atom	δ_{cal}	δ_{exp}
	NF-Urea			**NF**	
C21	49.2	48.1	C21	48.87	49.8
C14	117.7	116.8	C14	117.65	118.2
C12	119.9	121.2	C12	118.57	118.2
C17	129.1	134.1	C17	127.24	133.1
C19	154.4	150.4	C19	152.09	151.9
C11	156.6	152.0	C11	157.89	151.9
C16	161.1	154.0	C16	160.98	151.9
C31	161.5	162.1	C20	167.4	168.9
C20	166.9	168.5		**Urea**	
			C8	160.62	162.6

Table S12 Calculated local reactivity properties of the atoms of NF-urea (monomer + 3urea) using Hirshfeld derived charges.

Atom No.	f_k^+	S_k^+	ω_k^+	f_k^-	S_k^-	ω_k^-	f_k^0	S_k^0	ω_k^0
1 O	0.0062	0.0018	0.0494	0.0340	0.0097	0.2712	0.0201	0.0058	0.1603
2 O	0.0408	0.0117	0.3256	0.1330	0.0381	1.0604	0.0869	0.0249	0.6930
3 O	0.0187	0.0054	0.1495	0.1232	0.0353	0.9828	0.0710	0.0203	0.5661
4 O	0.0143	0.0041	0.1140	0.0318	0.0091	0.2535	0.0230	0.0066	0.1837
5 O	0.0233	0.0067	0.1861	0.0374	0.0107	0.2920	0.0303	0.0087	0.2420
6 N	0.0085	0.0024	0.0678	0.0718	0.0206	0.5730	0.0402	0.0115	0.3204
7 N	0.0182	0.0052	0.1451	0.0708	0.0203	0.5647	0.0445	0.0127	0.3549
8 N	0.0320	0.0091	0.2550	0.0177	0.0051	0.1413	0.0248	0.0071	0.1982
9 N	0.0087	0.0025	0.0693	0.0143	0.0041	0.1139	0.0115	0.0033	0.0916
10 H	0.0040	0.0011	0.0317	0.0083	0.0024	0.0666	0.0062	0.0018	0.0492
11 C	0.0178	0.0051	0.1422	0.0555	0.0159	0.4428	0.0367	0.0105	0.2925
12 C	0.0401	0.0115	0.3199	0.0455	0.0130	0.3629	0.0428	0.0123	0.3414
13 H	0.0186	0.0053	0.1484	0.0305	0.0087	0.2433	0.0245	0.0070	0.1958

14 C	0.0247	0.0071	0.1974	0.0658	0.0188	0.5247	0.0453	0.0130	0.3611
15 H	0.0165	0.0047	0.1319	0.0342	0.0098	0.2730	0.0254	0.0073	0.2025
16 C	0.0362	0.0104	0.2888	0.0343	0.0098	0.2734	0.0352	0.0101	0.2811
17 C	0.0318	0.0091	0.2537	0.0455	0.0130	0.3632	0.0387	0.0111	0.3085
18 H	0.0146	0.0042	0.1169	0.0268	0.0077	0.2139	0.0207	0.0059	0.1654
19 C	0.0084	0.0024	0.0673	0.0257	0.0073	0.2046	0.0170	0.0049	0.1359
20 C	0.0070	0.0020	0.0558	0.0131	0.0037	0.1045	0.0100	0.0029	0.0802
21 C	0.0092	0.0026	0.0737	0.0087	0.0025	0.0695	0.0090	0.0026	0.0716
22 H	0.0109	0.0031	0.0868	0.0092	0.0026	0.0731	0.0100	0.0029	0.0799
23 H	0.0146	0.0042	0.1161	0.0112	0.0032	0.0897	0.0129	0.0037	0.1029
24 O	0.0644	0.0184	0.5139	0.0173	0.0049	0.1377	0.0408	0.0117	0.3258
25 N	0.0121	0.0035	0.0968	−0.0075	−0.0021	−0.0594	0.0023	0.0007	0.0187
26 H	0.0121	0.0034	0.0962	−0.0001	−0.0000	−0.0004	0.0060	0.0017	0.0479
27 H	0.0050	0.0014	0.0397	−0.0092	−0.0026	−0.0735	−0.0021	−0.0006	−0.0169
28 N	0.0408	0.0117	0.3253	0.0018	0.0005	0.0143	0.0213	0.0061	0.1698
29 H	0.0093	0.0026	0.0739	0.0062	0.0018	0.0495	0.0077	0.0022	0.0617
30 H	0.0097	0.0028	0.0777	−0.0025	−0.0007	−0.0198	0.0036	0.0010	0.0290
31 C	0.0194	0.0055	0.1546	0.0039	0.0011	0.0309	0.0116	0.0033	0.0927
32 O	0.0230	0.0066	0.1838	−0.0009	−0.0002	−0.0070	0.0111	0.0032	0.0884
33 N	0.0247	0.0071	0.1968	0.0015	0.0004	0.0122	0.0131	0.0037	0.1045
34 H	0.0109	0.0031	0.0870	−0.0017	−0.0005	−0.0134	0.0046	0.0013	0.0368
35 H	0.0075	0.0022	0.0601	0.0017	0.0005	0.0134	0.0046	0.0013	0.0367
36 N	0.0493	0.0141	0.3932	0.0059	0.0017	0.0474	0.0276	0.0079	0.2203
37 H	0.0122	0.0035	0.0971	0.0029	0.0008	0.0230	0.0075	0.0021	0.0601
38 H	0.0155	0.0044	0.1236	0.0032	0.0009	0.0256	0.0093	0.0027	0.0746
39 C	0.0133	0.0038	0.1063	0.0012	0.0003	0.0097	0.0073	0.0021	0.0580
40 O	0.0539	0.0154	0.4302	0.0039	0.0011	0.0313	0.0289	0.0083	0.2308
41 N	0.0170	0.0049	0.1357	0.0015	0.0004	0.0118	0.0092	0.0026	0.0737
42 H	0.0147	0.0042	0.1174	0.0049	0.0014	0.0388	0.0098	0.0028	0.0781
43 H	0.0146	0.0042	0.1163	0.0028	0.0008	0.0221	0.0087	0.0025	0.0692
44 N	0.0403	0.0115	0.3217	−0.0009	−0.0003	−0.0072	0.0197	0.0057	0.1572
45 H	0.0075	0.0021	0.0597	−0.0014	−0.0004	−0.0111	0.0030	0.0009	0.0243
46 H	0.0157	0.0045	0.1251	−0.0011	−0.0003	−0.0089	0.0073	0.0021	0.0581
47 C	0.0187	0.0054	0.1495	0.0010	0.0003	0.0077	0.0098	0.0028	0.0786
48 O	−0.0061	−0.0018	−0.0490	−0.0053	−0.0015	−0.0420	−0.0057	−0.0016	−0.0455
49 N	0.0123	0.0035	0.0984	0.0056	0.0016	0.0443	0.0090	0.0026	0.0713
50 H	0.0061	0.0018	0.0490	0.0041	0.0012	0.0325	0.0051	0.0015	0.0408
51 H	0.0113	0.0032	0.0901	0.0057	0.0016	0.0458	0.0085	0.0024	0.0679
52 N	0.0156	0.0045	0.1248	0.0004	0.0001	0.0033	0.0080	0.0023	0.0640
53 H	0.0035	0.0010	0.0280	−0.0002	−0.0001	−0.0018	0.0016	0.0005	0.0131
54 H	0.0132	0.0038	0.1051	0.0047	0.0013	0.0374	0.0089	0.0026	0.0712
55 C	0.0067	0.0019	0.0539	0.0020	0.0006	0.0163	0.0044	0.0013	0.0351

Table S13 Calculated local reactivity properties of the atoms of NF-urea (monomer) using Hirshfeld derived charges.

Atom No.	f_k^+	S_k^+	ω_k^+	f_k^-	S_k^-	ω_k^-	f_k^0	S_k^0	ω_k^0
1 O	0.0026	0.0009	0.0228	0.0336	0.0115	0.2977	0.0181	0.0062	0.1603
2 O	0.0515	0.0176	0.4564	0.1263	0.0433	1.1204	0.0889	0.0304	0.7884
3 O	0.0141	0.0048	0.1250	0.1145	0.0392	1.0155	0.0643	0.0220	0.5703
4 O	0.0163	0.0056	0.1445	0.0388	0.0133	0.3441	0.0276	0.0094	0.2443
5 O	0.0401	0.0137	0.3555	0.0433	0.0148	0.3837	0.0417	0.0143	0.3696
6 N	0.0103	0.0035	0.0912	0.0697	0.0239	0.6179	0.0400	0.0137	0.3546
7 N	0.0211	0.0072	0.1870	0.0728	0.0249	0.6458	0.0469	0.0161	0.4164
8 N	0.0382	0.0131	0.3389	0.0163	0.0056	0.1448	0.0273	0.0093	0.2419
9 N	0.0151	0.0052	0.1336	0.0155	0.0053	0.1375	0.0153	0.0052	0.1356
10 H	0.0143	0.0049	0.1271	0.0174	0.0060	0.1543	0.0159	0.0054	0.1407
11 C	0.0253	0.0087	0.2246	0.0509	0.0174	0.4515	0.0381	0.0130	0.3381
12 C	0.0503	0.0172	0.4461	0.0482	0.0165	0.4276	0.0492	0.0169	0.4368
13 H	0.0243	0.0083	0.2152	0.0312	0.0107	0.2766	0.0277	0.0095	0.2459
14 C	0.0330	0.0113	0.2926	0.0613	0.0210	0.5439	0.0471	0.0161	0.4182
15 H	0.0212	0.0073	0.1882	0.0336	0.0115	0.2980	0.0274	0.0094	0.2431

16 C	0.0418	0.0143	0.3707	0.0368	0.0126	0.3262	0.0393	0.0134	0.3484
17 C	0.0324	0.0111	0.2878	0.0540	0.0185	0.4794	0.0432	0.0148	0.3836
18 H	0.0183	0.0063	0.1628	0.0288	0.0099	0.2558	0.0236	0.0081	0.2093
19 C	0.0135	0.0046	0.1197	0.0299	0.0102	0.2650	0.0217	0.0074	0.1923
20 C	0.0092	0.0031	0.0813	0.0155	0.0053	0.1378	0.0123	0.0042	0.1095
21 C	0.0107	0.0037	0.0950	0.0086	0.0029	0.0762	0.0096	0.0033	0.0856
22 H	0.0154	0.0053	0.1366	0.0109	0.0037	0.0967	0.0131	0.0045	0.1167
23 H	0.0138	0.0047	0.1221	0.0108	0.0037	0.0956	0.0123	0.0042	0.1089
24 O	0.1988	0.0681	1.7635	0.0197	0.0067	0.1744	0.1092	0.0374	0.9689
25 N	0.0592	0.0203	0.5248	−0.006	−0.0020	−0.0532	0.0266	0.0091	0.2358
26 H	0.0219	0.0075	0.1941	−0.0023	−0.0008	−0.0201	0.0098	0.0034	0.0870
27 H	0.0231	0.0079	0.2051	−0.0044	−0.0015	−0.0387	0.0094	0.0032	0.0832
28 N	0.0562	0.0192	0.4982	0.0042	0.0014	0.0374	0.0302	0.0103	0.2678
29 H	0.0314	0.0107	0.2784	0.0134	0.0046	0.1188	0.0224	0.0077	0.1986
30 H	0.0261	0.0089	0.2312	0.0024	0.0008	0.0213	0.0142	0.0049	0.1262
31 C	0.0507	0.0174	0.4499	0.0043	0.0015	0.0380	0.0275	0.0094	0.2439

Table S14 Calculated local reactivity properties of the atoms of NF using Hirshfeld derived charges.

Atom No.	f_k^+	S_k^+	ω_k^+	f_k^-	S_k^-	ω_k^-	f_k^0	S_k^0	ω_k^0
1 O	0.0715	0.0193	0.5135	0.5135	0.0096	0.2549	0.0535	0.0144	0.3842
2 O	0.2733	0.0737	1.9619	1.9619	0.0353	0.9410	0.2022	0.0545	1.4514
3 O	0.1986	0.0535	1.4254	1.4254	0.0340	0.9039	0.1623	0.0437	1.1647
4 O	0.3323	0.0896	2.3847	2.3847	0.0119	0.3157	0.1881	0.0507	1.3502
5 O	0.3021	0.0814	2.1678	2.1678	0.0115	0.3077	0.1725	0.0465	1.2378
6 N	−0.2200	−0.0593	−1.5787	−1.5787	0.0195	0.5188	−0.0738	−0.0199	−0.5299
7 N	0.1939	0.0523	1.3913	1.3913	0.0196	0.5226	0.1333	0.0359	0.9570
8 N	0.2481	0.0669	1.7807	1.7807	0.0048	0.1269	0.1329	0.0358	0.9538
9 N	0.1135	0.0306	0.8149	0.8149	0.0040	0.1073	0.0642	0.0173	0.4611
10 H	−0.1679	−0.0453	−1.2051	−1.2051	0.0048	0.1274	−0.0751	−0.0202	−0.5389
11 C	0.0083	0.0022	0.0595	0.0595	0.0143	0.3820	0.0308	0.0083	0.2207
12 C	0.1812	0.0488	1.3001	1.3001	0.0129	0.3440	0.1145	0.0309	0.8220
13 H	−0.0608	−0.0164	−0.4364	−0.4364	0.0086	0.2288	−0.0145	−0.0039	−0.1038
14 C	0.0491	0.0132	0.3524	0.3524	0.0173	0.4597	0.0566	0.0153	0.4061
15 H	−0.0779	−0.0210	−0.5588	−0.5588	0.0094	0.2515	−0.0214	−0.0058	−0.1536
16 C	0.0804	0.0217	0.5768	0.5768	0.0099	0.2642	0.0586	0.0158	0.4205
17 C	0.0525	0.0141	0.3770	0.3770	0.0137	0.3651	0.0517	0.0139	0.3710
18 H	−0.0497	−0.0134	−0.3565	−0.3565	0.0077	0.2056	−0.0105	−0.0028	−0.0754
19 C	−0.2264	−0.0610	−1.6249	−1.6249	0.0080	0.2138	−0.0983	−0.0265	−0.7056
20 C	−0.2010	−0.0542	−1.4422	−1.4422	0.0041	0.1096	−0.0928	−0.0250	−0.6663
21 C	0.0084	0.0023	0.0603	0.0603	0.0024	0.0648	0.0087	0.0023	0.0626
22 H	−0.0549	−0.0148	−0.3937	−0.3937	0.0030	0.0806	−0.0218	−0.0059	−0.1566
23 H	−0.0548	−0.0148	−0.3935	−0.3935	0.0030	0.0806	−0.0218	−0.0059	−0.1565

Table S15 Binding energies, inhibition constants and interaction energies of NF against protein targets of E. Coli. using Autodock 4.2.

Protein	Targets	Binding energy (kcal mol^{-1})	Inhibition costant Ki (μm)	Intermolecular energy (kcal mol^{-1})	Hydrogen bonds (Å) with binding sites
Hu Alpha2	1MULA	−4.89	260.95	−5.78	2.14 (N7) SerA 81
ELAV-like protein1	3HI9	−10.64	15.81	−11.54	2.36 (O5) AsnA 21 1.76 (H10) AsnA 21 2.26 (N7) SerA 48

					2.49 (O1) AlaA 49 2.35 (O2) ArgC 37 1.69 (O3) AlaA 49 1.71 (O3) ArgA 37
Glutaredoxin	IGRX	−6.09	34.56	−6.98	2.07 (O4) TyrA 35 1.68 (O3) LysA 18 2.07 (O3) ArgA 8
	1EGO	−5.56	84.72	−6.45	1.88 (H10) ThrA 73 2.03 (H10) AspA 74 2.26 (O5) ThrA 73
	5CAX	−8.26	886.31	−9.15	2.06 (O5) PheC 51 2.58 (O4) TyrB 49 1.90 (O3) LysC 10 1.66 (O2) AspC 7 2.21 (O2) ThrC 8
	2MZC	−6.59	14.78	−7.48	2.00 (H10) PheB 57 2.33 (O4) GlyB 53 2.14 (N7) GlyB 53 2.32 (O1) AsnB 55 1.77 (O3) ArgB 54 2.27 (O2) ArgA 21